People's Democratic Republic of Algeria
Ministry of Higher Education and Scientific Research
Kasdi Merbah University of Ouargla
Faculty of New Information and Communication Technologies
Department of Electronics and Telecommunications

Academic Master's thesis

Domain: Science and technology

Sector: Telecommunications

Option: Telecommunications System

Presented by:

- **Boubkeri sara mabrouka**
- **Benamara LiLia**

Theme:

Optimization and Evaluation of Channel Estimation Methods in Massive MIMO Systems for 5G/6G Communications

In front of the jury:

Mr. Aounallah Naceur	Supervisor	Professor, KMU Ouargla
Mr. Moad Mohamed Sayah	Président	MCA, KMU Ouargla
Mdm. Louazene hassiba	Examiner	MCB, KMU Ouargla
Mr. Labed Smail	Co-Supervisor	PhD student, KMU Ouargla

Academic Year: 2025/2026

بسم الله الرحمن الرحيم

Acknowledgement

Praise be to God, finally, praise befitting His glorious countenance and magnificent dominion, who granted us success and bestowed upon us the strength, patience, and determination to complete this work. By His grace and generosity, this thesis has been completed, and to Him, glory be to Him, belongs all praise and gratitude for His countless blessings.

We extend our deepest gratitude and appreciation to our supervisor, ***Professor Nasser Awnallah****, for his invaluable guidance, follow-up, sound advice, support, and full participation in this thesis. His scientific expertise and experience played a significant role in the successful completion of this work, and we offer him our sincere thanks and appreciation.*

We also extend our thanks to all the professors in the Electronics Department who contributed to the scientific and academic materials, enriching our university journey with their knowledge and expertise.

We must also express our deepest gratitude to our families, who were our greatest support and help, providing love, encouragement, and sacrifices that greatly contributed to our continued progress and the realization of this achievement.

Finally, we extend our thanks to everyone who contributed, directly or indirectly, to the completion of this scientific work, and for their assistance and support throughout this journey.

Thank you all ✍

DEDICATIONS I

In the name of Allah, the Most Gracious, the Most Merciful

To those whose prayers were the source of my strength, whose love inspired my determination, and whose support illuminated my path...
*To my **"beloved parents"**, who, after Allah Almighty, have been the reason behind every success I have achieved. They surrounded me with care, love, and unwavering support throughout every stage of my life. Words cannot adequately express my gratitude for their sacrifices and efforts. To them, I extend my deepest appreciation and respect, and I pray that Allah blesses them with health, happiness, and a long life.*

*To my **dear maternal aunt and my sister** , who has always been a source of encouragement and support through her kind words and constant motivation, I express my sincere gratitude and appreciation.*

*To my **loyal friends** whom I met during my university years, who shared with me moments of hardship before joy, and accompanied me throughout my journey with sincerity and devotion. They were a true source of support and companionship, and the memories we created together will remain among the most cherished memories of this stage of my life.*

*To those **special people** whose names are not written in these lines, yet who hold a special place in my heart, and whose presence and support left an unforgettable impact on this journey.*

I dedicate to all of you the fruit of this humble effort, praying that Allah grants success and prosperity in the steps that lie ahead.

Boubkeri Sara ✍

DEDICATIONS II

Praise be to Allah, by whose grace good deeds are done, and with Him the journeys are completed and wishes come true.

The journey was not short, nor should it have been. The dream was not near, and the road was not paved with ease. Yet, I walked it and reached its end.

To the one who adorned my name with the most beautiful titles, who supported me without limits and gave me endlessly without asking for anything in return.

To the one who taught me that perseverance is the weapon of knowledge and learning, my first supporter in my path, my strength and my refuge after God.
To my pride and honor,
My Father...

To the one for whom I pray that God places Paradise beneath her feet, who embraced me with her heart before her hands, who made hardships easier through her prayers, who was the light in times of darkness, and the candle that illuminated my darkest nights,
The secret of my strength and success,
My Mother...

To my steadfast support and source of safety, to those whose encouragement was for me a spring from which goodness flowed, the light of my eyes and the strength of my vision,
My Brother and Sisters...

To everyone who was a helping hand and support along this path, To those who stood beside me through hardships and crises, I dedicate to you this achievement and the fruit of a success I have long wished for. Today, I have completed and fulfilled the second of my aspirations by the grace of Almighty God. All praise is due to God for what I am and for what I have become.

Benamara LiLia ✍

Abstract

The evolution of wireless communication systems towards 5G and future 6G networks has been increasingly demanding in terms of higher data rates, ultra-low latency, enhanced reliability, and massive connectivity. Massive MIMO and its extension XL-MIMO have been developed as a key enabling technology to meet these requirements by improving spectral efficiency, coverage and system capacity. However, the performance of such systems is highly dependent on the availability of accurate Channel State Information (CSI). As the number of antennas increases and the wireless propagation environments become more complex, conventional channel estimation methods are confronted with the issues of high computational complexity, large pilot overhead and limited estimation accuracy. The work reviews and studies channel estimation techniques for Massive MIMO and XL-MIMO systems, with an emphasis on sparse channel estimation and optimization-based approaches. In particular, classical methods such as LS and LMMSE, as well as compressed sensing techniques such as OMP, CoSaMP, AMP, GAMP and SAMP, are reviewed. Moreover, the advanced estimation frameworks based on SOMP and ROMP are simulated in far-field, near-field and hybrid-field propagation environments. The obtained results show that the exploitation of channel sparsity can significantly improve the estimation accuracy and reduce the pilot overhead and computational burden. The results highlight the importance of optimised channel estimation strategies for reliable and efficient communications in future 5G and 6G wireless networks.

Keywords: Massive MIMO, XL-MIMO, 5G, 6G, Channel Estimation, CSI, Compressed Sensing, OMP, SOMP, ROMP, Optimization.

Résumé

Les technologies Massive MIMO et XL-MIMO jouent un rôle clé dans les systèmes modernes de télécommunications afin de répondre aux exigences croissantes des réseaux de communication sans fil de cinquième et sixième générations, notamment en matière de débit élevé, de faible latence, de fiabilité et de connectivité massive. Ces systèmes sont toutefois très dépendants de la précision de l'estimation du canal radio. L'augmentation du nombre d'antennes et la complexité des environnements de propagation rendent les méthodes conventionnelles d'estimation du canal limitées, du fait de leur complexité de calcul et de la surcharge des pilotes. Ce mémoire a pour objet l'étude et l'évaluation des principales techniques d'estimation de canal appliquées aux systèmes Massive MIMO et XL-MIMO. On étudie les méthodes classiques telles que LS et LMMSE ainsi que les approches basées sur le *Compressed Sensing* notamment OMP, CoSaMP, AMP, GAMP et SAMP. On s'intéresse tout particulièrement aux techniques qui exploitent la parcimonie des canaux sans fil ainsi qu'aux approches d'optimisation qui visent à améliorer les performances d'estimation. On réalise des simulations afin d'évaluer les performances des algorithmes SOMP et ROMP dans différents environnements de propagation (far-field, near-field et hybrid-field). Les résultats montrent que les méthodes qui exploitent la structure parcimonieuse du canal permettent d'améliorer de façon significative la précision de l'estimation tout en réduisant la surcharge des pilotes et la complexité de calcul. Cette étude souligne ainsi l'importance des techniques d'estimation optimisées pour les futurs systèmes de communication 5G et 6G.

Mots-clés : Massive MIMO, XL-MIMO, 5G, 6G, Estimation de canal, CSI, Compression de données, OMP, SOMP, ROMP, Optimisation.

الملخص

تتناول هذه المذكرة دراسة وتحسين وتقييم طرق تقدير القناة في أنظمة MIMO Massive وXL-MIMO الموجهة لشبكات الاتصالات اللاسلكية من الجيل الخامس (5G) والجيل السادس (6G). ومع التزايد المستمر في متطلبات معدلات نقل البيانات العالية، وزمن التأخير المنخفض، والموثوقية المرتفعة، والاتصال الكثيف بالأجهزة، أصبحت معرفة حالة القناة (CSI) بدقة عاملاً أساسياً لضمان الأداء الفعال لأنظمة الاتصالات الحديثة.

في البداية، تم عرض التطور الذي شهدته شبكات الاتصالات من الجيل الخامس إلى الجيل السادس، مع التركيز على دور تقنية MIMO Massive في تحسين الكفاءة الطيفية وزيادة سعة النظام وتحسين التغطية. كما تم التطرق إلى خصائص انتشار الإشارات اللاسلكية ونماذج القنوات المختلفة المستخدمة في بيئات الاتصالات الحديثة.

بعد ذلك، تمت دراسة أهم تقنيات تقدير القناة، بدءاً من الطرق التقليدية مثل LS وLMMSE، وصولاً إلى تقنيات الاستشعار المضغوط مثل OMP وCoSaMP وAMP وGAMP وSAMP، بالإضافة إلى أساليب التحسين والخوارزميات المعتمدة على التعلم الآلي.

وأخيراً، تم تقييم أداء خوارزميات SOMP وROMP في بيئات انتشار مختلفة، حيث أظهرت النتائج أن استغلال خاصية التشتت المحدود للقناة يساهم في تحسين دقة التقدير وتقليل التعقيد الحسابي وعدد الإشارات المرجعية المطلوبة.

الكلمات المفتاحية: Massive MIMO، XL-MIMO، 5G، 6G، تقدير القناة، CSI، الاستشعار المضغوط، OMP، SOMP، ROMP، التحسين.

Contents

1 Generalities On 5G And 6G Communication Networks **16**
- 1.1 Introduction . . . 16
- 1.2 Evolution From 5G To 6G Communication Systems . . . 16
- 1.3 New Performance Requirements . . . 17
  - 1.3.1 ULTRA- Reliability . . . 17
  - 1.3.2 Extreme Data Rates . . . 17
  - 1.3.3 Massive Connectivity . . . 17
- 1.4 Importance Of Accurate Channel Estimation In Massive MIMO . . . 18
- 1.5 Motivation For Optimization-oriented Approaches . . . 18
- 1.6 Massive MIMO In 5G And 6G Networks . . . 19
  - 1.6.1 Massive MIMO Architecture And Principles . . . 19
    - 1.6.1.1 Massive MIMO Architecture . . . 19
    - 1.6.1.2 Massive MIMO Principles . . . 20
  - 1.6.2 Differences Between 5G And Emerging 6G Scenarios . . . 22
  - 1.6.3 Role Of Massive MIMO At . . . 23
    - 1.6.3.1 Sub-6GHz . . . 23
    - 1.6.3.2 Mm Wave . . . 24
    - 1.6.3.3 Terahertz (THz) Bands . . . 24
- 1.7 Channel Characteristics And Models . . . 24
  - 1.7.1 Propagation Characteristics In 5G/6G Frequency Bands . . . 24
  - 1.7.2 Flat vs Frequency-Selective Fading . . . 25
    - 1.7.2.1 Flat Fading . . . 25
    - 1.7.2.2 Frequency Selective Fading . . . 26
  - 1.7.3 Rayleigh , Rician , And Sparse Channel Models . . . 27
    - 1.7.3.1 Rayleigh Channel Model . . . 27
    - 1.7.3.2 Rician Channel Model . . . 27
    - 1.7.3.3 Sparse Channel Models . . . 28
- 1.8 conclusion . . . 28

2 Channel Estimation And Optimization Techniques **30**
- 2.1 Introduction . . . 30
- 2.2 Classical Channel Estimation Methods . . . 30
  - 2.2.1 Least Squares (LS) . . . 31
  - 2.2.2 Linear Minimum Mean Square Error (LMMSE) . . . 32
- 2.3 Compressed Sensing-Based Channel Estimation . . . 32
  - 2.3.1 Orthogonal Matching Pursuit (OMP) . . . 33
    - 2.3.1.1 Advantages Of OMP . . . 35

2.3.1.2 Limitations of OMP . . . 35
2.3.2 Compressive Sampling Matching Pursuit (CoSaMP) . . . 35
2.3.2.1 Advantages Of CoSaMP . . . 37
2.3.3 Approximate Message Passing (AMP) . . . 37
2.3.3.1 Advantages Of AMP . . . 38
2.3.3.2 Limitations of AMP . . . 38
2.3.4 Generalized AMP (GAMP) . . . 38
2.3.4.1 Limitation Of GAMP . . . 40
2.3.4.2 Advantages Of GAMP . . . 40
2.3.5 Sparsity Adaptive Matching Pursuit (SAMP) . . . 41
2.3.5.1 Advantages Of SAMP . . . 43
2.3.5.2 Limitations Of SAMP . . . 43
2.4 Bayesian And Parametric Estimation Methods . . . 44
2.4.1 Bayesian Estimation . . . 44
2.4.2 Machine Learning And Deep Learning-Based Estimation . . . 44
2.4.2.1 Machine Learning . . . 44
2.4.2.2 Deep Learning Based Estimators . . . 44
2.4.3 Parametric Estimation Methods . . . 45
2.5 Channel Optimization Techniques . . . 46
2.5.1 Particle Swarm Optimization (PSO) . . . 46
2.5.1.1 Advantages Of PSO . . . 47
2.5.1.2 Limitations Of PSO . . . 48
2.5.2 Problem Formulation For Channel Estimation Optimization . . . 48
2.6 Optimization Objectives . . . 48
2.6.1 MSE Minimization . . . 48
2.7 Iterative And Low-Complexity Solvers . . . 49
2.8 Conclusion . . . 50

3 Simulation Results and Performance Evaluation 52
3.1 Introduction . . . 52
3.2 Channel Estimation in Different Fields for XL MIMO . . . 52
3.2.1 System and Signal Mode . . . 52
3.2.2 Channel Modeling Paradigms . . . 52
3.2.2.1 Far-Field Model . . . 53
3.2.2.2 Near-Field Model . . . 53
3.2.2.3 Hybrid-Field Model . . . 54
3.2.3 Nused Model SOMP-Based Estimation . . . 54
3.2.4 Simulation . . . 55
3.2.4.1 Result Analysis . . . 56
3.3 Exploiting Mixed LoS/NLoS Environments for Near-Field Channel Estimation in XL-MIMO Systems . . . 60
3.3.1 System and Signal Model . . . 61
3.3.2 Characterization of Mixed LoS/NLoS Near-Field Channels . . . 61
3.3.3 Rayleigh Distance Boundaries for Near-Field XL-MIMO . . . 62
3.3.4 Proposed Near-Field codebook based ROMP . . . 63
3.3.5 Proposed Far-Field codebook based ROMP . . . 64
3.3.6 Simulation . . . 66
3.3.6.1 Result Analysis . . . 66

3.4 Conclusion 69

List of Figures

1.1 Massive-MIMO basic architecture . . . 19
1.2 Massive MIMO uplink operation . . . 21
1.3 Massive MIMO down link operation . . . 21
1.4 Comparison between 5G and 6G communications. . . . 23
1.5 Flat fading . . . 25
1.6 Selective Fading . . . 26
1.7 Sparse channel with both precursor and postcursor components. . . . 28

2.1 Deep learning for channel estimation . . . 45

3.1 NMSE performance comparison with respect to the SNR. . . . 57
3.2 NMSE performance comparison with respect to the Number of Paths . . . 58
3.3 NMSE performance comparison with respect to the Pilot Overhead . . . 59
3.4 NMSE performance comparison with respect to the Sparsity Level . . . 59
3.5 NMSE performance comparison with respect to the Adjustable Parameter 60
3.6 Geometric structure of a near-field XL-MIMO system with both transmitter and receiver equipped by uniform linear arrays . . . 62
3.7 Definition of propagation regions: (a) Extreme near-field zone, (b) Transitional near-field zone, and (c) Conventional planar far-field zone . . . 63
3.8 Impact of Tx-Rx distance on NMSE performance in XL-MIMO fields. . . . 66
3.9 NMSE performance vs. SNR under an extreme near-field channel condition (Distance = 30 m, Pilot Length = 72). . . . 67
3.10 NMSE performance vs. SNR under a transitional near-field channel condition (Distance = 90 m, Pilot Length = 72). . . . 68
3.11 Impact of pilot overhead scaling on the estimation accuracy of OMP and proposed ROMP algorithms in XL-MIMO fields. . . . 68

List of Tables

3.1 Simulation Parameters 55

List of Abbreviations

5G:	Fifth Generation
6G:	Sixth Generation
ADC:	Analog-to-Digital Converter
AI:	Artificial Intelligence
AMP:	Approximate Message Passing
AoA:	Angle of Arrival
AoD:	Angle of Departure
AWGN:	Additive White Gaussian Noise
BP:	Basis Pursuit
BS:	Base Station
CoSaMP:	Compressive Sampling Matching Pursuit
CRLB:	Cramér–Rao Lower Bound
CS:	Compressed Sensing
CSI:	Channel State Information
DAC:	Digital-to-Analog Converter
DFT:	Discrete Fourier Transform
DSP:	Digital Signal Processing
HF-SOMP:	Hybrid-Field Simultaneous Orthogonal Matching Pursuit
IoT:	Internet of Things
IRS:	Intelligent Reflecting Surface
IRT:	Isochronous Real Time
ISI:	Inter-Symbol Interference
LMMSE:	Linear Minimum Mean Square Error
LoS:	Line-of-Sight
LS:	Least Squares
mMTC:	Massive Machine Type Communication
MIMO:	Multiple-Input Multiple-Output
MIMO-ARD:	MIMO Advanced Rayleigh Distance
MIMO-RD:	MIMO Rayleigh Distance
MMSE:	Minimum Mean Square Error
MMV:	Multiple Measurement Vector
mmWave:	Millimeter Wave
MSE:	Mean Square Error
NLoS:	Non-Line-of-Sight
NMSE:	Normalized Mean Square Error
OMP:	Orthogonal Matching Pursuit
PDF:	Probability Density Function
PSO:	Particle Swarm Optimization
RF:	Radio Frequency
ROMP:	Regularized Orthogonal Matching Pursuit
SAMP:	Sparsity Adaptive Matching Pursuit
SE:	Spectral Efficiency

SNR:	Signal-to-Noise Ratio
SOMP:	Simultaneous Orthogonal Matching Pursuit
THz:	Terahertz
TSN:	Time Sensitive Networking
UE:	User Equipment
ULA:	Uniform Linear Array
UM-MIMO:	Ultra-Massive Multiple-Input Multiple-Output
URLLC:	Ultra-Reliable Low-Latency Communication
XL-MIMO:	Extremely Large-Scale Multiple-Input Multiple-Output
ZF:	Zero Forcing

General Introduction

The increasing wireless communication systems have resulted in a growing demand for higher data rates, ultra-low latency, enhanced reliability and massive connectivity. To fulfil these demands, sophisticated technologies have been implemented in 5G networks, but 6G networks are expected to further advance communication capabilities through intelligent networking, terahertz communications, and ultra-massive antenna systems. Massive MIMO and its evolution towards XL-MIMO is one of the enabling technologies of modern wireless communications that has attracted a considerable attention due to its ability to improve spectral efficiency, coverage and system capacity.

However, the performance of Massive MIMO and XL-MIMO systems heavily relies on the availability of accurate Channel State Information (CSI). Accurate channel estimation becomes more challenging as the number of antennas increases and the wireless propagation environment becomes more complex, especially in the near-field and hybrid-field scenarios anticipated in future 6G systems. Traditional channel estimation approaches often suffer from significant computational complexity, excessive pilot overhead, and degraded performance in sparse and high-dimensional channel environments.

"Optimization-based methods and compressed sensing techniques have been proposed as promising approaches to address these challenges. Algorithms such as OMP, CoSaMP, AMP, GAMP, SAMP, etc. can significantly lower the estimation complexity by exploiting the inherent sparsity of wireless channels, and meanwhile obtain high estimation accuracy. Moreover, the recent developments in XL-MIMO systems call for novel estimation frameworks that can handle the near-field and far-field propagation characteristics.

The main aim of this dissertation is to study, analyse and evaluate the channel estimation methods for Massive MIMO and XL-MIMO systems in the context of 5G and future 6G communications. Special emphasis is placed on sparse channel estimation techniques and optimisation based approaches that improve estimation performance while maintaining a low pilot overhead and computational load.

The manuscript consists of three chapters. The first chapter deals with the fundamentals of 5G and 6G communication networks, Massive MIMO technology, wireless propagation characteristics, and channel models. Chapter 2 deals with the problems of channel estimation and optimisation techniques such as classical estimators, compressed sensing techniques, machine learning techniques and optimisation frameworks. Chapter 3 presents simulation results and performance evaluation of advanced channel estimation algorithms for XL-MIMO systems, including SOMP- and ROMP-based frameworks and a comparative study of their effectiveness in different propagation environments.

Chapter 1

Generalities on 5G and 6G Communication Networks

Chapter 1

Generalities On 5G And 6G Communication Networks

1.1 Introduction

Wireless communication systems are rapidly evolving from 5G toward 6G to support higher data rates, ultra-low latency, massive connectivity, and improved reliability. Technologies such as Massive MIMO, mmWave, THz communications, and beamforming have become critical to meet such requirements. However, the performance of these systems highly depends on the accurate channel estimation and efficient optimisation techniques.

In this chapter, we discuss the evolution from 5G to 6G networks and introduce the principles of Massive MIMO systems, beamforming techniques, and high-frequency communications. This chapter also describes wireless channel characteristics and common channel models which are important for channel estimation in future communication systems.

1.2 Evolution From 5G To 6G Communication Systems

The groundwork laid by 5G will be built upon and improved in 6G. The aim of 6G is to increase data rates by a factor of 10 to 100 compared to 5G. The delay-sensitive applications will benefit from the low latency of the system, and both system capacity and spectrum efficiency will be improved. The main driving force behind the development of 6G wireless technologies is to surpass the limitations of 5G.

In the future, the convergence of physical and digital worlds will pose further challenges for data communication. In this regard, several candidate technologies are studied, including those in the terahertz (THz) frequency range or based on artificial intelligence (AI). While the 6G experience is foreseen in the near future, the achievement of the 6G KPIs brings new problems to be researched extensively. Future smart cities will be able to operate independently from human intervention when data rates reach 1 Tbps . 6G networks are expected to bring at least 10Gbps speeds per client (and in some cases up to 100Gbps), compared to 1 Gbps in 5G. The sixth generation network performance can improve the frequency reuse by using flexible frequency sharing .

The 6th generation (6G) wireless communication network is planned to merge terrestrial, aerial and maritime communications into a single, unified system that is more

stable and faster, and can support a much larger number of devices with ultra-low latency requirements[1].

1.3 New Performance Requirements

1.3.1 ULTRA- Reliability

Ultra-reliable and low-latency communication (URLLC) in the fifth-generation (5G) communica-tion systems aims to meet the stringent reliability and latency requirements of mission and safety-critical applications . It requires characterising statistics of extreme and rare events (e.g., taming the tail of latency distribution) instead of average-based system designs.In the development of new applications, much more strict requirements on reliability and latency than those imposed in 5G URLLC are also required. In particular, 5-nine reliability and millisecond latency cannot be tolerated by high-precision robot control and autonomous ve-hicles. Factory automation over wire-less links should guarantee 7-nines reliability and sub-1 ms latency, similar to those of the Ethernet-based time sensitive networking (TSN) and isochronous realtime (IRT) system standards . Besides, the next generation (6G) wireless systems is facilitating 9-nine reliability with 0.1 ms latency for supporting intelligent systems based on different perceptual modalities (or Internet of senses) and real-time human-machine interactions [2] .

1.3.2 Extreme Data Rates

Consumers have been demanding higher and higher data rates since the beginning of telecommunication. 5G can transmit data at several gigabits per second, compared to the few kbps of 1G. 6G will actually work at a higher frequency to get more bandwidth, terahertz, visible light, etc. Future smart cities will be able to run without any human intervention when data rates reach 1 Tbps. For the upcoming 6G networks, the target data rate is 10 Gbps per client or even 100 Gbps, versus 1 Gbps in 5G.Flexible frequency sharing technology can be applied to frequency reuse to improve the performance of the sixth generation network [3].

1.3.3 Massive Connectivity

Another application of the cutting edge wireless technology is massive machine type communications (mMTC) . IoT here works without the interference of human. Machine-to-machine describes communication between electronic devices, such as telephone calls, text messages and command transmissions. The machines seem to be talking to each other, without any human intervention or interpretation of their instructions. It is expected that the density of mobile devices will reach 10^7 per square kilometre in the near future.Communication between these gadgets can be achieved using peer-to-peer and multi-hop cooperative relay technologies. Various communication network architectures require specialised software and hardware to cater to the diverse content driven applications and networks. This leads to the need for a new planning and optimisation strategy for next generation wireless networks [3].

1.4 Importance Of Accurate Channel Estimation In Massive MIMO

Channel estimation in massive MIMO is of significance to maintain high data rates and reliability due to the large number of antennas . Traditional channel estimation techniques may become computationally intensive and impractical . Therefore , advanced signal processing technique , and machine learning algorithms are employed to enhance channel estimation accuracy and reduce computational complexity . Another important aspect of Massive MIMO optimisation is beam forming. What it does is control the way signals are sent and received in specific directions to maximise signal quality and minimise interference. 5G networks can achieve high throughput and better resource utilisation by optimising beam forming techniques. Real time data driven adaptive beam forming algorithms are very important to adapt to the changed network conditions and user mobility [4].

1.5 Motivation For Optimization-oriented Approaches

Optimization-based approaches have become an essential solution to meet the rising complexity and performance demands of modern wireless communication systems, especially for massive MIMO, 5G, and beyond 6G networks[5] [7] . In large-scale antenna systems and highly dynamic propagation environments, conventional estimation and signal processing methods suffer from high computational complexity, limited scalability and accuracy degradation[7]. Hence the possibility to efficiently exploit sparsity, minimise the estimation errors, improve spectral efficiency and reduce energy consumption by mathematically rigours formulations motivates the optimisation based methods [6]. These approaches formulate communication tasks, e.g. channel estimation, beamforming, resource allocation and signal detection, as an optimisation problem, in which the objective functions are minimised or maximised under practical system constraints[5][6]. Furthermore, optimisation frameworks enable the integration of sophisticated techniques, including compressed sensing , convex optimisation , machine learning , and Bayesian inference , which improve robustness and flexibility in near-field and hybrid-field communication settings [6][8] . In future wireless systems that require ultra-reliable low-latency communication (URLLC), high data rates, and massive connectivity [7][8], optimization-oriented strategies are essential for reliable and computationally efficient system performance. Optimization-oriented approaches have been considered as a fundamental solution to cope with the increasing complexity and performance requirements of modern wireless communication systems, particularly in massive MIMO, 5G, and beyond 6G networks [5] [7]. Traditional estimation and signal processing methods are generally characterised by high computational complexity, limited scalability, and decreased accuracy in large-scale antenna systems and highly dynamic propagation environments [7]. Therefore, optimization-based methods are motivated by their ability to efficiently exploit sparsity, minimise estimation errors, improve spectral efficiency, and reduce energy consumption through mathematically rigorous formulations [6]. These approaches formulate communication tasks such as channel estimation, beamforming, resource allocation and signal detection as optimisation problems with objective functions to be minimised or maximised under practical system constraints [5] [6]. Moreover, optimisation frameworks allow the flexibility to utilise advanced techniques such as compressed sensing, convex optimisation,

machine learning, and Bayesian inference, which enhance robustness and adaptability in near-field and hybrid-field communication scenarios [6] [8]. With future wireless systems demanding ultra-reliable low-latency communication (URLLC), high data rates and massive connectivity, optimization-oriented strategies have become necessary to achieve reliable and computationally efficient system performance [7] [8].

1.6 Massive MIMO In 5G And 6G Networks

1.6.1 Massive MIMO Architecture And Principles

1.6.1.1 Massive MIMO Architecture

Massive MIMO is the most intriguing technology for 5G and beyond wireless access era. Massive MIMO is the evolution of the state-of-the-art MIMO systems deployed in the current wireless networks. Unlike conventional MIMO, massive MIMO utilizes a very large number of antennas at the base station, which can be in the order of tens to hundreds or even thousands, to serve multiple users simultaneously.The fundamental principle of massive MIMO is that a larger number of antennas enables the base station to focus the transmitted energy in smaller spatial regions. Therefore, the radiated beams are more spatially directed towards the intended users and are narrower. This spatial focusing leads to increased spectral efficiency, improved system throughput and significantly reduced interference to neighboring users. Larger antenna arrays produce more accurate beam patterns which in turn produce higher quality signals and more reliable transmission for the uplink and downlink.Architecture of a massive MI MO system consists of several critical components that work in concert to ensure efficient communication performance :

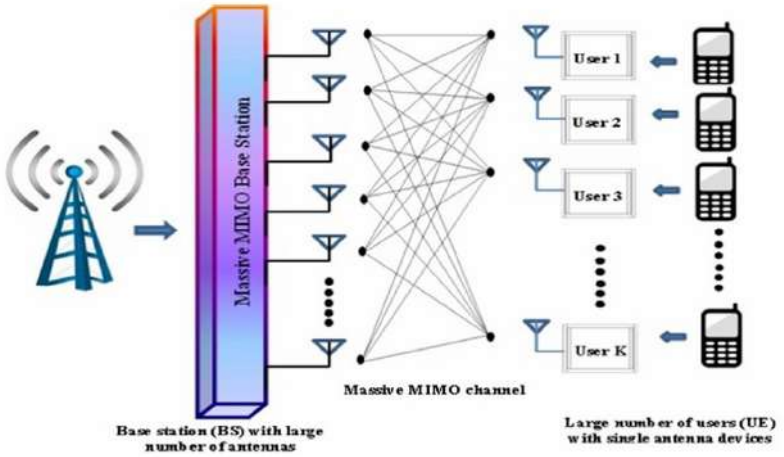


Figure 1.1: Massive-MIMO basic architecture

will note it below[9]:

1.Antenna Array: The key physical element of the massive MIMO system is the antenna array. It consists of a large number of antenna elements placed at the base station. The large scale array enables the system to utilize spatial diversity and array gain.Increasing the number of antennas allows the system to form highly directional beams

towards particular users. This capability improves the strength of received signals and lowers the interference between users sharing the same time and frequency resources.

2.RF Chains: Each antenna element is attached to a Radio Frequency (RF) chain. The RF chain performs the analog-to-digital and digital-to-analog conversion. It contains essential hardware components such as amplifiers, filters, mixers, digital to analog converters (DAC) and analog to digital converters (ADC).In massive MIMO systems that are fully digital, each antenna usually has one RF chain. However, the number of RF chains affects the system complexity, implementation cost and power consumption.

3. Digital Signal Processing Unit: The DSP unit is the computing heart of the big MIMO system. It performs all base band processing procedures required for transmission and reception of signals. The main processing operations are:

- **Channel Estimation:** Channel estimate is used to obtain accurate channel state information (CSI) between base station and consumers. This information is critical to perform effective beamforming and coherent detection of signals.

- **Precoding:** Precoding is employed in downlink transmission. It minimizes the interference between users by processing the transmitted signals so that they are directed towards the desired users.

- **Detection:** Detection is primarily performed in the uplink phase. A base station distinguishes and decodes signals simultaneously received from several users.

4.Beamforming System: Beamforming is an important technique in large MIMO systems. The base station can adjust phase and amplitude of signals throughout the antenna array so that it focuses energy on particular users, rather than broadcasting energy equally in all directions.The more antennas there are, the better the performance and the less interference there is. This is one of the key elements that differentiates huge MIMO from standard MIMO systems.

1.6.1.2 Massive MIMO Principles

Uplink and downlink are the two main transmission phases which comprise the operation of a big MIMO system. The two protocols describe the exchange of signals between users and the base station [9].

1. Uplink Transmission: Figure 1.2 shows the uplink channel which is used to send data and the pilot signal from the user terminal to the base station. Consider a massive MIMO uplink system where M antennas at the base station communicate with N ($M \gg N$) single antenna users concurrently.

If the signal sent by the user or deterministic pilot signal to estimate the channel is $x \in \mathbb{C}^N$, then the signal received at the base station in uplink is :

$$y = Hx + n_{\text{uplink}} \tag{1.1}$$

where $y \in \mathbb{C}^M$ is the signal received at the base station, H is the channel vector between the user terminal and the base station, and the elements of :

$$H \in \mathbb{C}^{M \times N}$$

are independent and identically distributed with zero mean and unit variance, i.e.,

$$H \sim \mathcal{CN}(0, 1)$$

The additional term $n_{\text{uplink}} \in \mathbb{C}^M$ is the sum of interference from several transmissions and the receiver noise. The additional interference is independent of the user signal x, but it can depend on the channel H.

$$n_{\text{uplink}} = n_{\text{noise}} + n_{\text{uplink-interference}} \tag{1.2}$$

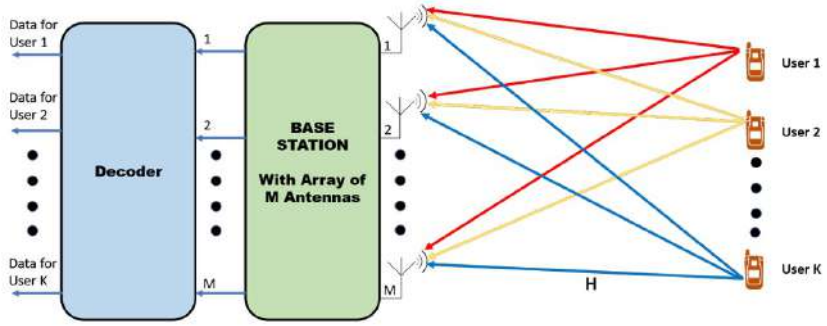


Figure 1.2: Massive MIMO uplink operation

2.Downlink Transmission: The downlink channel is used for data transmission or channel estimation between user and base station. The base station estimates the channel by using training pilots. Figure 1.3 shows a downlink transmission with multiple UE and a base station. Consider a downlink massive MIMO system where the base station is equipped with M antennas and serves N single antenna users at the same time.

The base station broadcasts independent information to multiple users simultaneously[9].

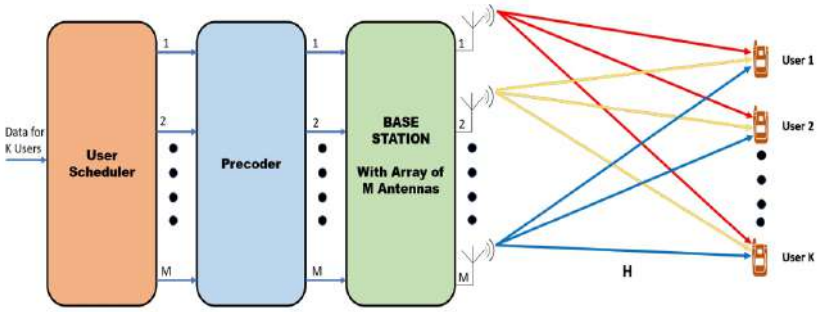


Figure 1.3: Massive MIMO down link operation

The k-th user receives the signal:

$$y_k = h_k x_k + n_{\text{downlink}} \tag{1.3}$$

where h_k denotes the channel vector between the k-th user and the base station, and the elements of h_k are i.i.d with zero mean and unit variance, i.e.,

$$h \sim \mathcal{CN}(0, 1)$$

$x_k \in \mathbb{C}^M$ is the signal transmitted by the base station for user k, and n_{downlink} is the additional noise which consists of the receiver noise

$$n_{\text{noise}} \sim \mathcal{CN}(0, \sigma^2 I)$$

And the interference during downlink $n_{\text{downlink-interference}}$ caused by transmitting simultaneously to other users and is given as :

$$n_{\text{downlink}} = n_{\text{downlink-interference}} + n_{\text{noise}} \tag{1.4}$$

1.6.2 Differences Between 5G And Emerging 6G Scenarios

The transition from fifth-generation (5G) to sixth-generation (6G) wireless networks represents a significant technological advancement rather than a simple upgrade. Compared to 5G, 6G is expected to substantially improve core performance metrics, including peak data rates, latency, spectrum utilization, connection density, and energy efficiency. For instance, while 5G supports peak data rates in the range of tens of gigabits per second and latency around 1 ms, 6G networks are projected to achieve peak rates up to 1 terabit per second (Tbps) and ultra-low latency on the order of tens of microseconds. Moreover, 6G will operate over broader frequency bands, extending into the terahertz (THz) spectrum, enabling significantly higher capacity and throughput. Alongside these enhancements, 6G is anticipated to support enhanced mobility, more reliable connectivity with higher device densities, and advanced network intelligence through ubiquitous integration of artificial intelligence (AI) and machine learning, addressing limitations in 5G for future data-intensive and ultra-reliable applications. Such comprehensive improvements underscore the paradigm shift expected with 6G in comparison to 5G.

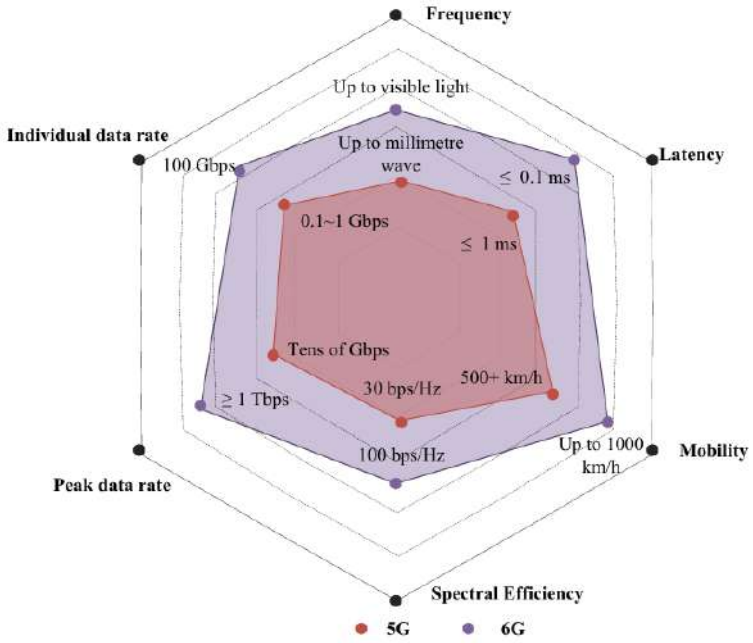


Figure 1.4: Comparison between 5G and 6G communications.

To achieve such stringent performance requirements, advanced physical layer technologies such as Massive MIMO are essential for both 5G and the emerging 6G systems. Massive MIMO improves spectral efficiency, capacity and energy efficiency by employing spatial multiplexing and beamforming techniques using a large number of antennas. Moreover, the transition to higher frequency bands and ultra-dense connectivity in 6G scenarios further amplifies the complexity of the channel, necessitating precise and optimised channel estimation methods to guarantee reliable and efficient communication performance [10].

1.6.3 Role Of Massive MIMO At

1.6.3.1 Sub-6GHz

• **Increased Spectral Efficiency:** Massive MIMO enables multiple users to share the same frequency band simultaneously, greatly improving spectral efficiency. This is particularly important for Sub-6 GHz systems with limited bandwidth.

• **Improved Signal Quality:** Beamforming steers signals directly to the intended users, improving the signal-to-noise ratio (SNR) and minimising the interference among users.

• **Higher Data Rates:** To increase the achievable data rates, massive MIMO supports multiple parallel data streams (spatial multiplexing). These rates are better in Sub-6 GHz but still lower than the targeted rates in mmWave or future 6G systems.

• **Enhanced Coverage:** Large antenna arrays help to propagate the signal so that even in difficult environments such as urban or rural areas, coverage can be relied upon.

• **Energy Efficiency:** Beamforming directs transmission energy only where it is needed, thus reducing total energy usage.

• **Interference Reduction :** Spatial separation among users helps in reducing the inter-user interference, which is critical in dense Sub-6 GHz networks.

• **Support For Massive Connectivity :** Massive MIMO allows serving a large number of users simultaneously, making it suitable for high density scenarios[11].

1.6.3.2 Mm Wave

The mmWave and massive MIMO technologies can be combined to satisfy the demands of future 5G networks. This technological combination of massive MIMO and mmWave systems have led to the emergence of mmWave-massive MIMO that provides a wide range of advantages: (a) multiplexing and array gains enabled by the large number of transmit and receive antennas, (b) extreme data rates enabled by the large bandwidth available at millimetre frequencies and (c) reduced interference enabled by the narrow beamforming[12].

1.6.3.3 Terahertz (THz) Bands

Terahertz (THz) communications at the 0.1-10 THz frequency band are promising to enable the next generation of high-speed wireless systems. The THz signals have the availability of extremely wide bandwidths in the order of tens of GHz, but suffer from large free-space spreading loss and molecular absorption, which severely limits their transmission distances. To address these propagation issues, ultra-massive multiple-input multiple-output (UM-MIMO) systems can be employed to produce highly directional beams with high gain by applying advanced beamforming schemes.This work presents an overview of beamforming technologies for THz UM-MIMO systems. First, the system model is introduced along with the associated channel characteristics and architectural configurations. Then the basic concepts of beamforming using UM-MIMO are described including the far-field and near-field propagation considerations. The paper also presents the beam training as a promising beamforming approach in the THz band, focusing on the training protocols and codebook design techniques. The research also investigates intelligent reflecting surface (IRS)-assisted joint beamforming as well as multi-user beamforming techniques in THz UM-MIMO systems. Moreover, spatial-wideband and frequency-wideband effects in THz beamforming are investigated and possible mitigation techniques are presented. Finally, fabrication technologies, emerging application scenarios and open research challenges in THz UM-MIMO systems are discussed [13].

1.7 Channel Characteristics And Models

1.7.1 Propagation Characteristics In 5G/6G Frequency Bands

In modern wireless communication systems, especially for 5G and beyond 6G technologies, the propagation characteristics are heavily altered by employing higher frequency

bands such as millimeter-wave (mmWave) and terahertz (THz) spectra. Unlike conventional sub-6 GHz systems, these frequency bands have unique and often difficult propagation characteristics. Propagation loss increases substantially at mmWave and THz bands, in particular, due to increased free-space attenuation, reduced ability for diffraction and increased susceptibility to environmental factors. As a result, signals are highly affected by blockage effects, where obstacles such as buildings, foliage, and even human bodies can cause significant attenuation, often requiring line-of-sight (LOS) communication links. Furthermore, atmospheric conditions have a greater impact at these frequencies, as rain, fog, humidity, and atmospheric gases cause additional absorption losses, which considerably degrade the signal strength, particularly in the THz bands where molecular absorption is a major factor. Also, the propagation environment is characterised by limited diffraction and enhanced scattering, which modifies the multipath structure of the channel and affects the reliability of the signal in non-line-of-sight (NLOS) conditions. Mobility performance is also affected by Doppler spread that is more pronounced at higher frequencies due to the proportionality between carrier frequency and Doppler shift. These combined effects result in highly directional short-range communication links that demand sophisticated techniques such as beamforming and dense deployment of base stations, in order to provide reliable connectivity. Hence, understanding the propagation characteristics of mmWave and THz frequency bands is crucial for designing and optimising next generation 5G and 6G wireless systems [14] .

1.7.2 Flat vs Frequency-Selective Fading

1.7.2.1 Flat Fading

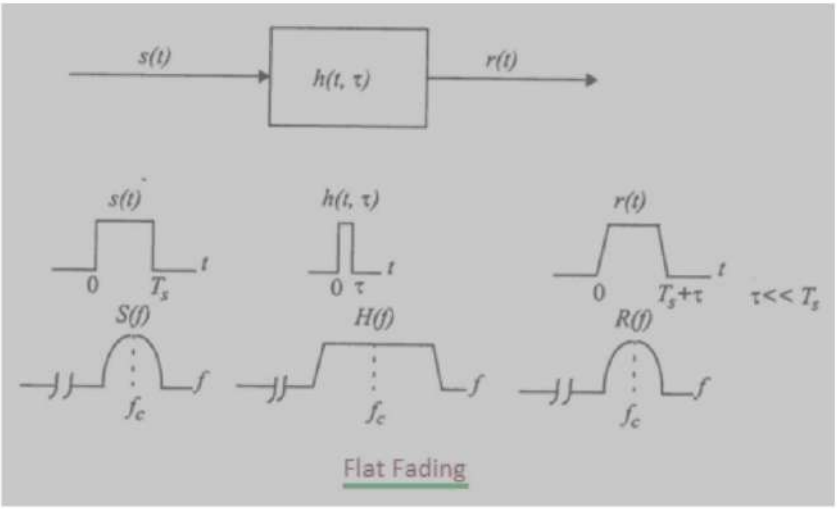


Figure 1.5: Flat fading

In the case of flat fading, the channel response is a linear phase and a constant gain over a bandwidth larger than the signal bandwidth. This implies that the spectral features of the transmitted signal are preserved over time without distortion in its frequency components. Such behaviour is illustrated in Fig 1.5, which shows the time-domain and frequency-domain representation of a flat fading channel.

Flat fading channels are sometimes called amplitude-varying channels because the amplitude of the signal changes with time but the spectral shape of the signal does not. In general they are also called narrowband channels because the signal bandwidth is much smaller than the channel bandwidth.

When the channel coherence bandwidth is greater than the signal bandwidth, the channel condition is the same for all frequencies of the transmitted signal, i.e. over the signal bandwidth the channel frequency response is essentially flat, hence the name Flat Fading. This corresponds to an expected less than signal symbol period in the time domain.

The notion of flat fading is used to describe the case when the signal bandwidth is much smaller than the channel coherence bandwidth ($B_s \ll B_c$) and the symbol duration is much larger than the delay spread ($T_s \gg \sigma_\tau$) [15][16].

1.7.2.2 Frequency Selective Fading

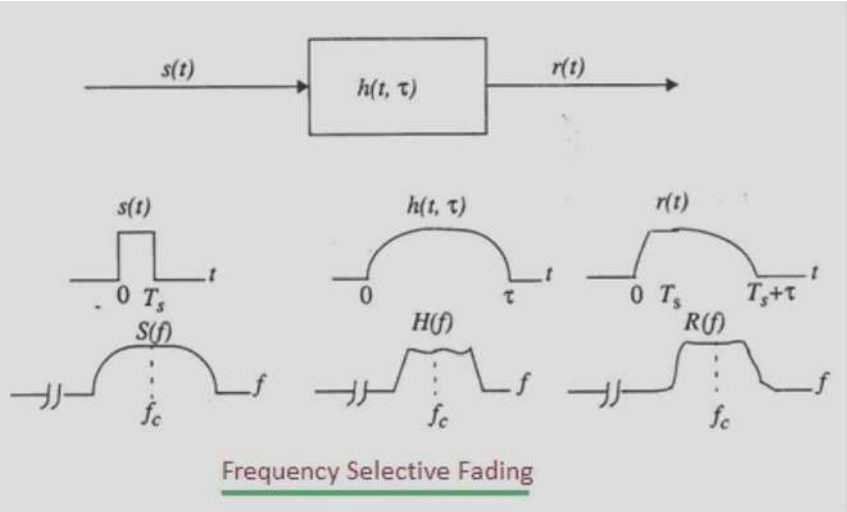


Figure 1.6: Selective Fading

In frequency selective fading the channel response is not flat over the bandwidth of the signal, and thus different frequencies of the transmitted signal will experience different gains and phase shifts. This happens when the channel bandwidth is less than the signal bandwidth. On the other hand if the channel bandwidth is smaller than the signal bandwidth, different frequency bands of the signal are affected differently. As a result the signal is distorted by inter-symbol interference (ISI) in which the received signal is made up of several delayed and attenuated copies of the transmitted waveform. Figure 6 illustrates this behaviour - the time- and frequencydomain characteristics of a frequency-selective fading channel.

Frequency selective fading occurs when the bandwidth of the signal is greater than the coherence bandwidth of the channel ($B_s > B_c$) and the symbol duration is less than the delay spread ($T_s < \sigma_{tau}$). The time domain analogue is that the channel is longer than the signal symbol period. It has been roughly estimated that a channel can be considered frequency-selective if the symbol duration is on the order or less than ten times the delay spread ($T_s \leq 10\sigma_\tau$) [15][16].

- The distinction between flat fading and frequency-selective fading can be demonstrated by means of parameters such as bandwidth and delay spread. In flat fading the

signal bandwidth is less than the channel bandwidth. All the frequency components are affected equally. The attenuation is uniform and does not cause spectral distortion. On the other hand , frequency-selective fading occurs when the signal bandwidth is greater than the channel bandwidth , resulting in differential attenuation and phase shifts of the frequency components . In the time domain, flat fading has a delay spread less than the symbol duration and so it does not cause inter-symbol interference (ISI). Frequency selective fading has a delay spread greater than the symbol duration which results in ISI and distortion of the signal. In flat fading channel, image is very badly degraded by random noise and block noise. In frequency selective fading channel, image is very badly degraded by random noise and inter-symbol interference (ISI) [15][16].

1.7.3 Rayleigh , Rician , And Sparse Channel Models

1.7.3.1 Rayleigh Channel Model

This model is employed when no direct line-of-sight (LOS) exists between the transmitter and the receiver. It is by far the most commonly used model due to its analytical simplicity. For this model, the distribution of the received power follows an exponential distribution. The model is obtained by letting $m_x = m_y = 0$ and $\sigma_x = \sigma_y = \sigma$. The PDF, CDF, and MGF of the SNR γ in this fading model are given by[17]:

$$f_\gamma(x) = \frac{1}{2\sigma^2} e^{-\frac{x}{2\sigma^2}} \tag{1.5}$$

$$F_\gamma(x) = 1 - e^{-\frac{x}{2\sigma^2}} \tag{1.6}$$

$$M_\gamma(s) = \frac{1}{1 - 2\sigma^2 s} \tag{1.7}$$

1.7.3.2 Rician Channel Model

Here, the in-phase and/or quadrature components of the received signal are modelled as Gaussian random variables with nonzero mean, thus accounting for the existence of a direct line-of-sight (LOS) path between the transmitter and the receiver, i.e., the specular component. The Rician fading model is a typical way to characterise such environments.However, the analysis of the Rician model is more complicated than that of the Rayleigh model because of the involvement of special transcendental functions. Namely, its probability density function (PDF) contains the modified Bessel function and its cumulative distribution function (CDF) includes the Marcum Q-function. The model parameters are such that the variances of the in-phase and quadrature components are equal, i.e. $\sigma_x = \sigma_y = \sigma$, while at least one of the mean values is non-zero, i.e. $m_x \neq 0$ and/or $m_y \neq 0$.The PDF, CDF and moment generating function (MGF) of this model are given below:

$$f_Y(x) = \frac{1}{2\sigma^2} \exp\left(-\frac{x + \nu^2}{2\sigma^2}\right) I_0\left(\frac{\nu\sqrt{x}}{\sigma^2}\right) \tag{1.8}$$

$$F_Y(x) = \sum_{k=0}^{\infty} \left(\frac{\nu^2}{2\sigma^2}\right)^k \exp\left(-\frac{\nu^2}{2\sigma^2}\right) \gamma\left(k+1, \frac{x}{2\sigma^2}\right) \tag{1.9}$$

$$M_Y(s) = \frac{\exp\left(\frac{\nu^2 s}{1-2\sigma^2 s}\right)}{1-2\sigma^2 s} \tag{1.10}$$

where $\nu = \sqrt{m_x^2 + m_y^2}$ and $K = \frac{\nu^2}{2\sigma^2}$ represent the channel parameters. Here, $I_0(\cdot)$ denotes the modified Bessel function of the first kind of order zero, while $\gamma(\cdot,\cdot)$ represents the lower incomplete Gamma function [17].

1.7.3.3 Sparse Channel Models

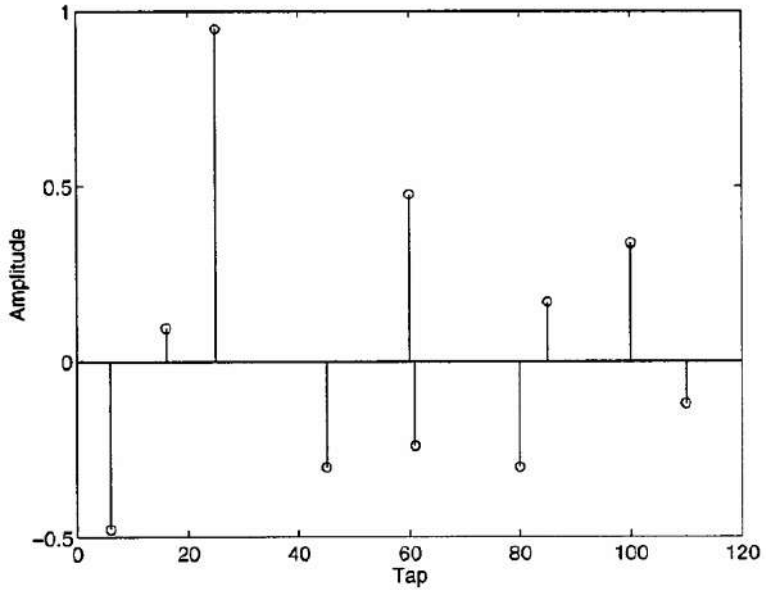


Figure 1.7: Sparse channel with both precursor and postcursor components.

Channels of this type, illustrated in Fig 1.7 , are characterized by a sparse impulse response and appear in various communication scenarios. For example, in high-definition television (HDTV), only a limited number of echoes are present, although the channel extends over a large number of symbol intervals. In broadband wireless systems, the so-called hilly terrain (HT) delay profile is associated with sparsely distributed multipath components. Similar behavior is also observed in underwater acoustic communication channels [18].

1.8 conclusion

This chapter introduced main concepts and enabling technologies of 5G and emerging 6G wireless communication systems. They discussed the architecture and principles of Massive MIMO, beamforming methods and high frequency communication bands. Also, the propagation characteristics and various wireless channel models are introduced.

The discussed concepts provide the theoretical background for understanding the challenges of channel estimation and importance of optimisation based approaches in Massive MIMO systems studied in the next chapters.

Chapter 2

Channel Estimation and Optimization Techniques

Chapter 2

Channel Estimation And Optimization Techniques

2.1 Introduction

Channel estimation and optimisation are two of the most important aspects in modern wireless communication systems, especially in the Massive MIMO and XL-MIMO technologies foreseen for 5G and 6G networks. Accurate channel state information (CSI) plays a key role in reliable signal detection, beamforming, resource allocation, and interference management. However, the large number of antennas and the high-dimensional nature of wireless channels pose considerable challenges in terms of computational complexity, pilot overhead and estimation accuracy.

In this chapter, we comprehensively review the channel estimation techniques and optimisation methods used in large scale antenna systems. Firstly, classical estimation methods such as Least Squares (LS) and Linear Minimum Mean Square Error (LMMSE) are presented. Then, compressed sensing based methods such as OMP, CoSaMP, AMP, GAMP, and SAMP are reviewed as the efficient solutions for sparse channel estimation. In this chapter, we also review Bayesian and parametric estimation techniques and newer machine learning and deep learning based approaches which have shown promise in complex wireless environments. Besides, different channel optimisation techniques such as PSO, radio resource optimisation and beamforming optimisation are surveyed. Finally, we analyse applications of these methods in Massive MIMO and XL-MIMO systems, optimisation objectives and low-complexity iterative solvers.

2.2 Classical Channel Estimation Methods

Channel estimation is the accurate estimation of the channel matrix (H) between transmitter and receiver. Channel estimation is required for precoding and detection and beamforming and other operations. The aim is to estimate the characteristics of the channel for a better accuracy of the signal transmission and reception. The process of channel estimation for the massive MIMO systems is to estimate the channel matrix(H) through the received signal$y$, the transmitted signal$x$ and the known pilot symbols or training sequences.

There are a number of factors such as system design, resources available and performance requirements that may influence the choice of algorithm and technique of channel

estimation. Some typical channel estimation methods in massive MIMO systems are [19] :

2.2.1 Least Squares (LS)

This method estimates the channel matrix by minimising the square of the difference between the received signal and the estimated signal. The LS estimator is simple and straightforward, but may be sensitive to noise and interference.

The relationship between transmitted and received signals can be modelled for the n-th time slot and m-th subcarrier as:

$$Y_{m,n} = H_{m,n} \times X_{m,n} + N_{m,n} \tag{2.1}$$

where $Y_{m,n}$ is the received signal, $X_{m,n}$ is the transmitted signal, $H_{m,n}$ is the channel response, and $N_{m,n}$ is the noise. The overall channel is represented by the matrix H, which spans all time slots and subcarriers.

In this context, the received signal Y is known and part of the transmitted signal X is also known due to the use of reference (pilot) signals. However, both channel H and noise N are unknown. Hence, channel estimation aims to recover H using the available information from Y and the known pilot symbols.

In an ideal noise-free scenario, the channel response at the pilot locations can be directly obtained as:

$$h_r = \frac{y_r}{x_r} \tag{2.2}$$

Where h_r, y_r, and x_r correspond to the channel response, received pilot signal, and transmitted pilot signal, respectively.

However, in real systems, noise cannot be neglected. Hence, the estimation problem is formulated as an optimisation problem, in which the objective is to minimise the difference between the received signal and the reconstructed signal. If the squared Euclidean norm is used as the optimisation criterion, the problem results in the Least Squares (LS) estimator.

The solution of this optimisation problem results in:

$$\hat{H}_r^{LS} = \text{diag}\left(\hat{H}_r^{LS}\right) = \frac{y_r}{x_r} \tag{2.3}$$

Although the LS estimator is simple and has low computational complexity, it only provides the channel estimates at pilot positions. To obtain the channel response over the entire time-frequency grid, the use of interpolation techniques is required.

A more sophisticated method is the Minimum Mean Square Error (MMSE) estimator. This estimator improves the estimation accuracy by using statistical information about the channel and noise. Particularly, the MMSE estimate is derived by filtering the LS estimate with a matrix.

However, this approach requires prior knowledge of the channel correlation and noise statistics, which are often difficult to obtain in practice. Moreover, the MMSE estimator has increased computational complexity and longer processing time, which limits its practical implementation in real-time systems[19].

2.2.2 Linear Minimum Mean Square Error (LMMSE)

We consider a narrowband point-to-point MIMO system with N_t transmit and N_r receive antennas. The propagation links are modelled as flat Rayleigh fading channels, which are slowly varying in time so that they can be considered constant during the transmission of L consecutive pilot symbols from each transmit antenna. For the training phase the input-output signal model may be expressed as [20]:

$$Y = HX + N \tag{2.4}$$

where Y is the $N_r \times L$ received signal matrix, X is the $N_t \times L$ complex matrix containing the information symbols and H is the $N_r \times N_t$ channel matrix. N is the $N_r \times L$ matrix of additive white Gaussian noise (AWGN) with independent zero-mean circularly-symmetric complex Gaussian entries with variance σ_n^2.

$$XX^\dagger = cLI_{N_t} \tag{2.5}$$

In this paper we are interested in LMMSE channel estimation. It is shown in it by information-theoretical means that for transmissions over spatially uncorrelated channels, LMMSE estimation performances are optimised by using training sequences X that are a multiple of a matrix with orthogonal columns [20].

$$\mathrm{tr}\left(XX^\dagger\right) = cLN_t \tag{2.6}$$

Where $\mathrm{tr}\left(XX^\dagger\right) = cLN_t$ is a power value depending on the adopted modulation format and transmit power constraint, with $c \in \mathbb{R}$.

In the more general case with spatial correlation, the optimal training sequences and per-antenna transmit powers should be optimised considering the spatial correlation matrices. However, here we assume that the transmitter has no knowledge on either channel state or channel correlation features. Hence, training sequences are drawn to satisfy (5)[20]. Also, we set :

$$L = N_t \tag{2.7}$$

Which is the minimum L such that the number of measurements is equal to the number of parameters to be estimated,

$$XX^\dagger = X^\dagger X = cN_t I_{N_t} \tag{2.8}$$

A shorter training sequence may provide a smaller estimation MSE, but at the cost of a reduced spectral efficiency. On the other hand, such a selection is optimal in many cases of interest.

We define the average SNR per receive antenna as as $\rho = \frac{\kappa}{\sigma_n^2}$, where $\kappa = cN_t$[20] .

2.3 Compressed Sensing-Based Channel Estimation

Compressive Sensing (CS) has been successfully applied to a wide range of signal processing applications, and in the case of imaging systems the technique has reached a high level of maturity. However its applications in wireless communications are still limited. One of the most important and widely studied area is channel estimation. One of the

significant applications of CS in wireless systems is sparse channel estimation for ultra-wideband communications. The motivation behind this application is that CS techniques can be applied to detect and recover individual propagation paths or clusters of multipath components in sparse wireless channels. The use of compressive sensing in channel estimation is motivated by the observation that many wireless channels have sparse multipath characteristics. In such channels the number of dominant propagation paths is much smaller than the total number of channel taps in the baseband representation. Exploiting this sparsity, compressive sensing methods can recover the channel with a small number of pilot symbols while achieving high estimation accuracy. Sparse multipath channels are usually modelled by assuming that most of the channel taps are negligible and only a few taps contain significant information. However, the sparsity level depends strongly on the threshold used to decide whether a channel tap is negligible or not. In addition, using an over-sampled baseband channel model may increase the ambiguity of the channel representation, but it is often more sparse, which can be further advantageous for compressive sensing based channel estimation methods [21].

2.3.1 Orthogonal Matching Pursuit (OMP)

Orthogonal Matching Pursuit (OMP) is a greedy algorithm, widely used in compression sensing and sparse channel estimation techniques [22][23]. The basic idea of OMP is to iteratively select the most correlated column with the residual of the received signal to reconstruct a sparse signal[22]. At each step, the algorithm finds the atom in the dictionary that has the maximum correlation with the current residual and updates the estimate of the signal by an orthogonal projection [22][23] . The appealing feature of OMP is its low computational complexity and ease of implementation . However, its performance deteriorates with increasing noise levels or when the dictionary columns are highly correlated . In Massive MIMO and XL-MIMO systems, the OMP is widely used to exploit the spatial sparsity of the channel to reduce driver overhead and improve spectral efficiency [23].

Algorithm 1 OMP for Signal Recovery

INPUT:

- An $N \times d$ measurement matrix Φ
- An N-dimensional data vector v
- The sparsity level m of the ideal signal

OUTPUT:

- An estimate $\hat{s}$ in $\mathbb{R}^d$ for the ideal signal
- A set Λ_m containing m elements from $\{1, \ldots, d\}$
- An N-dimensional approximation a_m of the data vector v
- An N-dimensional residual $r_m = v - a_m$

PROCEDURE:

1. Initialize the residual $r_0 = v$, the index set $\Lambda_0 = \emptyset$, and the iteration counter $t = 1$.
2. Find the index λ_t that solves the easy optimization problem
$$\lambda_t = \arg\max_{j=1,\ldots,d} |\langle r_{t-1}, \varphi_j \rangle| .$$
If the maximum occurs for multiple indices, break the tie deterministically.
3. Augment the index set
$$\Lambda_t = \Lambda_{t-1} \cup \{\lambda_t\}$$
and the matrix of chosen atoms
$$\Phi_t = \begin{bmatrix} \Phi_{t-1} & \varphi_{\lambda_t} \end{bmatrix} .$$
We use the convention that Φ_0 is an empty matrix.
4. Solve a least-squares problem to obtain a new signal estimate:
$$x_t = \arg\min_x \|\Phi_t x - v\|_2.$$
5. Calculate the new approximation of the data and the new residual:
$$a_t = \Phi_t x_t,$$
$$r_t = v - a_t.$$
6. Increment t, and return to Step 2 if $t \leq m$.
7. The estimate $\hat{s}$ for the ideal signal has nonzero indices at the components listed in Λ_m. The value of the estimate $\hat{s}$ in component λ_j equals the jth component of x_m.

The OMP model based on compressed sensing can be written as:

$$\mathbf{y} = \mathbf{x} + \mathbf{n} \tag{2.9}$$

OMP in each iteration chooses the column which has the maximum correlation to the residual vector [23]:

$$\lambda_t = \arg\max_j |\langle r_{t-1}, \phi_j \rangle| \tag{2.10}$$

The algorithm proceeds to update the signal estimate with a least squares optimisation step and computes a new residual. The iterative process is repeated until a stopping criterion is satisfied, e.g., a predefined sparsity level or a minimised reconstruction error.

2.3.1.1 Advantages Of OMP

- Low computational complexity in comparison with convex optimisation methods such as Basis Pursuit (BP) [22].
- Fast convergence and efficient implementation in practical systems [23].
- Accurate sparse signal reconstruction with reduced number of measurements[22] .
- Reduced pilot overhead for Massive MIMO and mmWave communication systems [22].
- Applicable to compressed sensing and sparse channel estimation applications[22] .
- Simple recursive implementation with iterative updates[23] .

2.3.1.2 Limitations of OMP

- Sensitive to noise and channel estimation error[22] .
- If the columns of the sensing matrix are highly correlated, performance degrades [23].
- Many applications require prior knowledge of the sparsity level [22].
- Reconstruction performance degrades in dense scattering environments [22] .
- Not as good as some advanced convex optimisation algorithms in highly complex scenarios[22].
- The accuracy can degrade when the signal is not exactly sparse [22].

2.3.2 Compressive Sampling Matching Pursuit (CoSaMP)

Compressive Sampling Matching Pursuit (CoSaMP) is an iterative algorithm that improves the performance of classical greedy algorithms such as OMP [24][25]. Unlike OMP that selects one atom at each iteration, CoSaMP selects multiple significant components simultaneously, which accelerates the convergence and improves the reconstruction accuracy [24].

The algorithm consists of several steps: identification of the dominant support, merging of the supports, least-squares estimation, and updating of the residual [24]. CoSaMP is robust to noise and it allows efficient reconstruction of sparse signals with a moderate complexity [24][25]. It is used in modern communication systems for channel estimation, signal detection and compressed sensing applications [25].

Algorithm 2 CoSaMP recovery algorithm

CoSaMP(Φ, u, s)
Input: Sampling matrix Φ, noisy sample vector u, sparsity level s
Output: An s-sparse approximation a of the target signal

$$a^0 \leftarrow 0 \qquad \text{(Trivial initial approximation)}$$

$$v \leftarrow u \qquad \text{(Current samples = input samples)}$$

$$k \leftarrow 0$$

repeat

$$k \leftarrow k + 1$$

$$y \leftarrow \Phi^* v \qquad \text{(Form signal proxy)}$$

$$\Omega \leftarrow \text{supp}(y_{2s}) \qquad \text{(Identify large components)}$$

$$T \leftarrow \Omega \cup \text{supp}(a^{k-1}) \qquad \text{(Merge supports)}$$

$$b|_T \leftarrow \Phi_T^{\dagger} u \qquad \text{(Signal estimation by least-squares)}$$

$$b|_{T^c} \leftarrow 0$$

$$a^k \leftarrow b_s \qquad \text{(Prune to obtain next approximation)}$$

$$v \leftarrow u - \Phi a^k \qquad \text{(Update current samples)}$$

until halting criterion true

The CoSaMP algorithm starts with the proxy computation step to find out the important components of the signal from the current residual. This step can be expressed as:

$$y = \Phi^* v \tag{2.11}$$

where v is the current residual and Φ^* is the conjugate transpose of the measurement matrix.

Then, the algorithm does support identification, by selecting the largest components of the proxy signal according to:

$$\Omega = \text{supp}(y_{2s}) \tag{2.12}$$

where supp is the support of the signal and $2s$ are the indices of the largest values.

Then CoSaMP merges the newly detected components with the previously estimated components by support merging:

$$T = \Omega \cup \text{supp}(a^{k-1}) \tag{2.13}$$

Then the algorithm performs least squares estimation to reconstruct the signal on the obtained support set:

$$b_T = \Phi_T^{\dagger} u \tag{2.14}$$

where $\Phi_T^{\dagger}$ is the Moore–Penrose pseudoinverse.
Then the pruning step retains the s largest components:

$$a^k = b_s \tag{2.15}$$

Finally, the residual is updated for the next iteration with:

$$v = u - \Phi a^k \tag{2.16}$$

This process is repeated iteratively until an accurate approximation of the original signal is obtained [25].

2.3.2.1 Advantages Of CoSaMP

-Rapid reconstruction.
-High precision.
-Low computational complexity.
-Robustness to noise.
-Suitable for compressible signals [24].

2.3.3 Approximate Message Passing (AMP)

The Approximate Message Passing (AMP) algorithm was introduced to solve sparse linear inverse problems in compressive sensing [26]. In massive MIMO systems, AMP is employed for channel estimation by leveraging the sparsity of wireless propagation channels. Taking the received pilot signal model :

$$\mathbf{y} = \mathbf{h} + \mathbf{n},$$

Where $\mathbf{y}$ is the received pilot observations, is the pilot sensing matrix, $\mathbf{h}$ is the sparse channel vector to be estimated and $\mathbf{n}$ is the additive white Gaussian noise.

The AMP algorithm iteratively builds the channel vector through a number of residual updates and denoising operations. Algorithm 1 summarises the channel estimation procedure based on AMP.

Algorithm 3 AMP-Based Channel Estimation

1: **Input:** $\mathbf{y}$, $,\sigma^2$
2: **Initialization:** $\hat{\mathbf{h}}^{(0)} = \mathbf{0}$, $\mathbf{r}^{(0)} = \mathbf{y}$
3: **for** $t = 1, \ldots, T$ **do**
4:
$$\mathbf{z}^{(t)} = \hat{\mathbf{h}}^{(t-1)} + {}^{H}\mathbf{r}^{(t-1)}$$
5:
$$\hat{\mathbf{h}}^{(t)} = \eta\big(\mathbf{z}^{(t)}\big)$$
6:
$$\mathbf{r}^{(t)} = \mathbf{y} - \hat{\mathbf{h}}^{(t)} + \frac{1}{M}\mathbf{r}^{(t-1)} \left\langle \eta'\big(\mathbf{z}^{(t)}\big) \right\rangle$$
7: **end for**
8: **Output:** $\hat{\mathbf{h}}$

AMP updates the channel estimate and residual error at each iteration until convergence. The algorithm can accurately recover the channel state information (CSI) from a limited number of pilot observations by leveraging the channel sparsity.

2.3.3.1 Advantages Of AMP

- Low computational complexity.
- Simple to implement in practice.
- Matrix-vector multiplication only.
- Efficient for sparse channel estimation in massive MIMO systems[26].

2.3.3.2 Limitations of AMP

- Works well when the assumptions of AMP are satisfied by the sensing matrix.
- The equivalent AWGN assumption is only asymptotically valid as the system dimensions grow very large.
- Performance loss due to model mismatch in practical channel estimation scenarios.
- Convergence is not guaranteed for arbitrary sensing matrix[26].

2.3.4 Generalized AMP (GAMP)

generalised approximate message passing or GAMP, which separates a vector-valued estimation problem into a sequence of scalar problems and linear transforms."The GAMP algorithm is a generalisation of several earlier Gaussian and quadratic approximations of loopy belief propagation (loopy BP) that have been successful in many previous applications, including, most recently, compressive sensing.The algorithm is based on the same idea as the AMP method: the vector-valued estimation problem is solved iteratively by a sequence of scalar operations on the input and output nodes.The scalar operations in the GAMP algorithm are defined by two functions, gout($\cdot$) and gin($\cdot$), which we refer to as the scalar estimation functions [27].

Algorithm 4 Generalized AMP (GAMP)

1: Given a matrix $A \in \mathbb{R}^{m \times n}$, system inputs and outputs q and y and scalar estimation functions $g_{in}(\cdot)$ and $g_{out}(\cdot)$, generate a sequence of estimates $\hat{\mathbf{x}}(t)$, $\hat{\mathbf{z}}(t)$ for $t = 0, 1, \ldots$

2: **Initialization:** Set $t = 0$ and set $\hat{x}_j(t)$ and $\tau_j^x(t)$ to some initial values.

3: **Output linear step:** For each i, compute

$$\tau_i^p(t) = \sum_j |a_{ij}|^2 \tau_j^x(t) \tag{5a}$$

$$\hat{p}_i(t) = \sum_j a_{ij}\hat{x}_j(t) - \tau_i^p(t)\hat{s}_i(t-1) \tag{5b}$$

$$\hat{z}_i(t) = \sum_j a_{ij}\hat{x}_j(t) \tag{5c}$$

where initially, we take $\hat{s}(-1) = 0$.

4: **Output nonlinear step:** For each i,

$$\hat{s}_i(t) = g_{out}(t, \hat{p}_i(t), y_i, \tau_i^p(t)) \tag{6a}$$

$$\tau_i^s(t) = -\frac{\partial}{\partial \hat{p}} g_{out}(t, \hat{p}_i(t), y_i, \tau_i^p(t)) \tag{6b}$$

5: **Input linear step:** For each j,

$$\tau_j^r(t) = \left[\sum_i |a_{ij}|^2 \tau_i^s(t)\right]^{-1} \tag{7a}$$

$$\hat{r}_j(t) = \hat{x}_j(t) + \tau_j^r(t) \sum_i a_{ij}\hat{s}_i(t) \tag{7b}$$

6: **Input nonlinear step:** For each j,

$$\hat{x}_j(t+1) = g_{in}\big(t, \hat{r}_j(t), q_j, \tau_j^r(t)\big) \tag{8a}$$

$$\tau_j^x(t+1) = \tau_j^r(t) \frac{\partial}{\partial \hat{r}} g_{in}\big(t, \hat{r}_j(t), q_j, \tau_j^r(t)\big) \tag{8b}$$

7: Increment $t = t + 1$ and return to step 2 until a sufficient number of iterations have been performed.

The Generalized Approximate Message Passing (GAMP) algorithm is defined through the following equations:

Output Linear Step

$$\tau_{p_i}^{(t)} = \sum_j |a_{ij}|^2 \tau_{x_j}^{(t)} \tag{2.17}$$

$$p_i^{(t)} = \sum_j a_{ij} x_j^{(t)} - \tau_{p_i}^{(t)} s_i^{(t-1)} \tag{2.18}$$

$$z_i^{(t)} = \sum_j a_{ij} x_j^{(t)} \tag{2.19}$$

Output Nonlinear Step

$$s_i^{(t)} = g_{out}\left(t, p_i^{(t)}, y_i, \tau_{p_i}^{(t)}\right) \tag{2.20}$$

$$\tau_{s_i}^{(t)} = -\frac{\partial}{\partial p} g_{out}\left(t, p_i^{(t)}, y_i, \tau_{p_i}^{(t)}\right) \tag{2.21}$$

Input Linear Step

$$\tau_{r_j}^{(t)} = \left(\sum_i |a_{ij}|^2 \tau_{s_i}^{(t)}\right)^{-1} \tag{2.22}$$

$$r_j^{(t)} = x_j^{(t)} + \tau_{r_j}^{(t)} \sum_i a_{ij} s_i^{(t)} \tag{2.23}$$

Input Nonlinear Step

$$x_j^{(t+1)} = g_{in}\left(t, r_j^{(t)}, q_j, \tau_{r_j}^{(t)}\right) \tag{2.24}$$

$$\tau_{x_j}^{(t+1)} = \tau_{r_j}^{(t)} \frac{\partial}{\partial r} g_{in}\left(t, r_j^{(t)}, q_j, \tau_{r_j}^{(t)}\right) \tag{2.25}$$

2.3.4.1 Limitation Of GAMP

-The matrix A couples or mixes the coefficients of x into z.
-The posterior distribution involves high-dimensional integrals that are difficult to evaluate.
-GAMP provides an approximate implementation of loopy belief propagation.
-The asymptotic analysis is derived for large Gaussian i.i.d. transform matrices.
-The State Evolution analysis is based on the large-system limit ($M, N \to \infty$) [27].

2.3.4.2 Advantages Of GAMP

-Holds for essentially arbitrary priors $P_{X|Q}$ and $P_{Y|Z}$.
-Arbitrary non-Gaussian input is manageable.
-Can handle output nonlinearities.
-Can implement approximations of both:

- MAP inference by max-sum loopy BP.
- Loopy BP for MMSE estimation and posterior marginals (sum-product).

-Simple to calculate.
-Each iteration consists only of scalar estimation computations and linear transforms.
-Similar in form to the fastest known methods of solving such problems.
-Excellent convergence in a few iterations.
-Usually converges in 10–20 iterations.
-Allows a simple scalar equivalent model for large Gaussian i.i.d. matrices.
-Performance is predicted by State Evolution (SE) equations.
-State Evolution can asymptotically predict metrics such as:

- Mean Square Error (MSE).
- Accuracy of Detection.

-Computationally feasible and widely applicable [27].

2.3.5 Sparsity Adaptive Matching Pursuit (SAMP)

A greedy compressed sensing reconstruction algorithm, Sparsity Adaptive Matching Pursuit (SAMP), is proposed to recover sparse signals when the sparsity level K is not known a priori. Unlike OMP and CoSaMP, SAMP estimates the support size adaptively during the reconstruction process, making it suitable for practical applications where the sparsity is unknown a priori.

Architecture for sparse signal recovery without prior knowledge of the sparsity level. The process starts with the acquisition of compressed measurements via a sensing matrix. The support set is then initialised as empty and the initial residual equal to the measurement vector is established. In each iteration, the algorithm selects the most relevant atoms by computing the correlation between the residue and the columns of the sensing matrix. The selected atoms are combined with the current support set and a least-squares estimation is performed to obtain an updated signal approximation. The residual is then recalculated as the difference between the measured signal and the reconstructed signal. The algorithm adapts the support size with the change of the residual energy, and increases the step length when needed. The procedure is repeated until a stopping criterion is reached, e.g. when the residual is sufficiently small or when the maximum number of iterations is reached. This adaptive architecture allows SAMP to efficiently recover sparse signals and automatically estimate the unknown sparsity level, making it applicable to practical compressed sensing applications. [28]

Algorithm 5 SAMP

Require: Compressed signal y, perception matrix A, step size S
Ensure: Signal sparse representation coefficient estimate $\hat{\theta}_t$

Initialization:
$r_0 = y$; $\Lambda_t = \emptyset$; $A_t = \emptyset$; $L = S$; $stage = 1$; $t = 1$
repeat
  $S_t = \mathrm{Max}\left(|A^T r_{t-1}|, L\right)$
  $C_t = \Lambda_{t-1} \cup S_t$
  $\hat{\theta}_t = \arg\min \|y - A_t\theta_t\| = (A_t^T A_t)^{-1} A_t^T y$
  $F_t = \max\left(\|A_t y\|, L\right)$
  $r_{\text{new}} = y - A_{tL}(A_{tL}^T A_{tL})^{-1} A_{tL}^T y$
  if $\|r_{\text{new}}\|_2 < 10^{-6}$ **then**
    Output θ_t
  else if $\|r_{\text{new}}\|_2 \geq \|r_{t-1}\|_2$ **then**
    $stage = stage + 1$
    $L = stage \times S$
    $t = t + 1$
  else
    $r_{\text{new}} = r_{t-1}$
    $\Lambda_t = F$
    $t = t + 1$
  end if
until $\|r_{\text{new}}\|_2 < 10^{-6}$
Output:
$\hat{\theta}_t = (A_t^T A_t)^{-1} A_t^T y$

Consider the compressed sensing model

$$y = \Phi x \tag{2.26}$$

where the sparse signal x can be represented as

$$x = \sum_{i=1}^{N} \Psi_i \theta_i = \Psi\theta. \tag{2.27}$$

Thus, the measurement process can be written as

$$y = \Phi x = \Phi\Psi\theta = A\theta, \tag{2.28}$$

where

$$A = \Phi\Psi \tag{2.29}$$

is the sensing matrix.
The sparse recovery problem aims to solve

$$\min_{\theta} \|\theta\|_0 \quad \text{subject to} \quad y = \Phi x, \tag{2.30}$$

while its practical convex relaxation is given by

$$\min_{\theta} \|\theta\|_1 \quad \text{subject to} \quad y = \Phi x. \tag{2.31}$$

In the SAMP algorithm, the initialization is performed as

$$r_0 = y, \qquad F_0 = \emptyset, \qquad L = S. \tag{2.32}$$

At iteration t, the algorithm selects the candidate atoms using

$$S_t = \max\left(|A^T r_{t-1}|, L\right), \tag{2.33}$$

and updates the candidate support set according to

$$C_t = \Lambda_{t-1} \cup S_t. \tag{2.34}$$

Subsequently, the signal estimate is obtained through the least-squares solution

$$\hat{\theta}_t = \arg\min_{\theta_t} \|y - A_t\theta_t\| = (A_t^T A_t)^{-1} A_t^T y. \tag{2.35}$$

The new residual is then computed as

$$r_{\text{new}} = y - A_{tL}(A_{tL}^T A_{tL})^{-1} A_{tL}^T y. \tag{2.36}$$

and the reconstructed measurement vector is given by

$$y_{tL} = y - r_{\text{new}} = A_{tL}(A_{tL}^T A_{tL})^{-1} A_{tL}^T y. \tag{2.37}$$

These iterative steps are repeated until the stopping criterion is satisfied, allowing the SAMP algorithm to recover sparse signals without requiring prior knowledge of the sparsity level.

2.3.5.1 Advantages Of SAMP

- Does not require prior knowledge of sparsity K.
- Adaptive support estimation.
- Lower computational complexity than l_1-minimization methods.
- Suitable for practical compressed sensing applications.
- Good reconstruction accuracy under noisy measurements.
- Can reconstruct signals with unknown sparsity levels [28].

2.3.5.2 Limitations Of SAMP

- Reconstruction quality depends on the selected step size.
- Convergence may be slower than CoSaMP when sparsity is known.
- Performance degrades at very low measurement rates.
- Sensitive to noise accumulation.
- More iterations may be required compared to OMP for some signals.
- Reconstruction error can increase if support updates are inaccurate [28].

2.4 Bayesian And Parametric Estimation Methods

2.4.1 Bayesian Estimation

Bayesian estimation methods are statistical techniques that leverage the prior knowledge of the wireless channel along with the observed received signals to improve the estimation accuracy. Bayesian approaches are very useful in wireless communication systems, especially massive MIMO and XL-MIMO systems, since they exploit the statistical properties of the channel, noise and sparsity. In the Bayesian setting, the channel coefficients are modelled as random variables and are estimated by maximising the posterior probability distribution based on the Bayes' rule. These methods are especially valuable in millimeter-wave (mmWave) and terahertz (THz) communication systems with sparse propagation environments. The Bayesian estimation techniques include Maximum A Posteriori (MAP), Minimum Mean Square Error (MMSE), Sparse Bayesian Learning (SBL) and Bayesian Compressive Sensing (BCS). Compared with conventional estimation methods, the Bayesian methods usually have better estimation accuracy and robustness under low signal-to-noise ratio (SNR) conditions, though generally they involve higher computational complexity due to iterative optimisation procedures [29][30].

$$P(H \mid Y) = \frac{P(Y \mid H)\, P(H)}{P(Y)} \tag{2.38}$$

2.4.2 Machine Learning And Deep Learning-Based Estimation

2.4.2.1 Machine Learning

Machine Learning (ML) is a subfield of Artificial Intelligence (AI) that allows systems to learn from data and improve their performance without being explicitly programmed. It is based on finding patterns and structures within large data sets to make predictions or informed decisions. ML techniques are generally divided into supervised, unsupervised and reinforcement learning. In wireless communications, ML has been attracting increasing attention in tasks such as channel estimation in which traditional techniques may fail in complex scenarios. Neural Networks (NNs) as a key component of ML consist of interconnected layers of artificial neurones that process information using activation functions. Among these, feed- forward neural networks are widely used for learning nonlinear mappings from inputs to outputs. Moreover, Convolutional Neural Networks (CNNs) have been successfully applied in channel estimation due to their ability to capture spatial features and extract meaningful representations from data. These properties make them especially suitable for modelling wireless channel characteristics and improving the estimation accuracy [19].

2.4.2.2 Deep Learning Based Estimators

Recently, deep learning-based channel estimation has become a promising alternative to conventional linear Channel State Information (CSI) estimation techniques, especially for the purposes of dimensionality reduction and estimation accuracy. A DNN-based framework was proposed to accurately estimate CSI and reduce pilot feedback overhead in this regard. This method was validated with ray-tracing simulations and showed considerable enhancement in the overall performance of wireless communication systems.

The suggested architecture was intended for an ultra-dense network (UDN) environment consisting of one macro base station (MBS) and multiple small base stations (SBSs). Likewise, another deep learning-based channel estimation scheme integrated with superimposed coding (SC) was proposed to reduce CSI feedback overhead further. The key idea of this method is to overlay the downlink CSI over uplink user data prior to transmission. At the base station (BS), the uplink data and downlink CSI are jointly reconstructed, followed by interference cancellation via iterative MMSE-based processing. Moreover, the proposed scheme adopts a subnet-by-subnet training strategy to accelerate convergence and ease parameter optimisation. The simulation results showed that this approach enhances CSI estimation performance in 5G massive MIMO systems, while maintaining efficient uplink bandwidth utilisation [31].

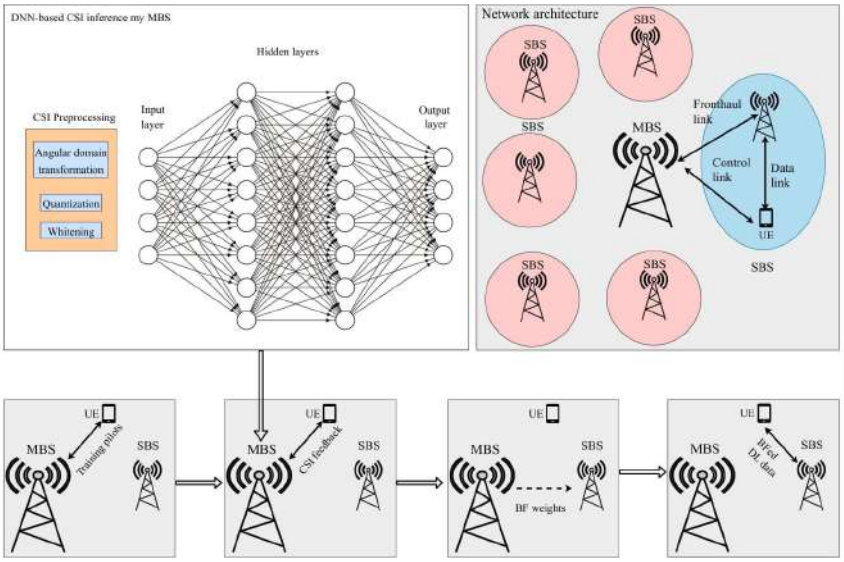


Figure 2.1: Deep learning for channel estimation

2.4.3 Parametric Estimation Methods

Parametric estimation approaches model the wireless channel using a finite set of physical parameters instead of estimating every channel coefficient independently. In these approaches, the channel is modelled by a structured model, which is defined by parameters such as angles of arrival (AoA), angles of departure (AoD), delays, path gains, etc. Such a representation can greatly reduce the dimensionality of the estimation problem and improve the estimation efficiency, especially in massive MIMO and millimeter-wave systems [32][33].

A popular parametric channel model is

$$H = \sum_{l=1}^{L} \alpha_l \, a_r(\theta_l) \, a_t^H(\phi_l) \tag{2.39}$$

L is the number of propagation paths, α_l is the complex gain of the l^{th} path, $a_r(\theta_l)$ and $a_t(\phi_l)$ are the array response vectors at the receiver and transmitter, respectively.

Then the estimation is performed by estimating these physical parameters based on subspace methods (MUSIC, ESPRIT), maximum likelihood estimation or compressed sensing based methods [34][35].

Parametric methods are especially useful in sparse propagation environments and are popular in next generation communication systems due to their lower complexity and high resolution [36][33].

2.5 Channel Optimization Techniques

The objective of channel optimisation techniques is to enhance the efficiency and reliability of wireless communication systems by increasing the accuracy of channel estimation, maximising system capacity, and minimising interference and error rates. These techniques are of special importance in modern communication systems such as massive MIMO, millimeter-wave (mmWave) and 5G/6G networks where the channel conditions are highly dynamic and complex [37].

- **MMSE (Mean Square Error Minimum):**
  - Reduces the channel estimation error between the true and estimated channel.
  - Utilizes statistical knowledge of channel and noise.
  - Better than LS, especially at low SNR [37].
- **Convex optimisation techniques:**
  - Express channel estimation as an optimisation problem.
  - Exploiting sparsity via ℓ_1-norm minimisation and LASSO.
  - Highly effective in mmWave and massive MIMO systems [38].
- **Iterative Methods:**
  - Iterative enhancement of channel estimates.
  - Include EM (Expectation-Maximization), gradient descent and coordinate descent.
  - Helpful when dealing with noisy or incomplete data [39].
- **Optimisation using machine learning:**
  - Uses neural networks and deep learning models.
  - Learns channel structure directly from the data.
  - Good performance in complex and changing environments [40].

2.5.1 Particle Swarm Optimization (PSO)

He Particle Swarm Optimization (PSO) is a population-based probabilistic optimisation technique inspired by the social behaviour of bird flocking and fish schooling. Originally proposed by Kennedy and Eberhart in 1995. PSO is an algorithm in which a swarm of particles search the optimal solution by updating their position based on their own and neighbour particle's experience [41].

PSO Architecture

Each particle can be described by three vectors:

-Present position: x_i

-Velocity: v_i
-Best personal position: p_i

The swarm also keeps the best solution found by the neighbourhood or the whole swarm, p_g. In each iteration, the particles evaluate the objective function, update their personal best positions and move towards promising regions of the search space [41].

PSO Flow

-Randomly initialise particles.
-Assess fitness.
-Update personal best (p_i).
-Update global best (p_g).
-Velocity update.
-Position update.
-Repeat until a stopping condition is reached [41].

Algorithm 6 Original PSO

Initialize a population array of particles with random positions and velocities on D dimensions in the search space.

loop

For each particle, evaluate the desired optimization fitness function in D variables.

Compare particle's fitness evaluation with its $pbest_i$. If current value is better than $pbest_i$, then set $pbest_i$ equal to the current value, and $\vec{p}_i$ equal to the current location $\vec{x}_i$ in D-dimensional space.

Identify the particle in the neighborhood with the best success so far, and assign its index to the variable g.

Change the velocity and position of the particle according to the following equations:

$$\vec{v}_i \leftarrow \vec{v}_i + \vec{U}(0, \phi_1) \otimes (\vec{p}_i - \vec{x}_i) + \vec{U}(0, \phi_2) \otimes (\vec{p}_g - \vec{x}_i)$$

$$\vec{x}_i \leftarrow \vec{x}_i + \vec{v}_i$$

If a criterion is met (usually a sufficiently good fitness or a maximum number of iterations), exit loop.

end loop

Notes:

– $\vec{U}(0, \phi_i)$ represents a vector of random numbers uniformly distributed in $[0, \phi_i]$ which is randomly generated at each iteration and for each particle.
– $\otimes$ is component-wise multiplication.
– In the original version of PSO, each component of $\vec{v}_i$ is kept within the range $[-V_{\max}, +V_{\max}]$.

2.5.1.1 Advantages Of PSO

The survey highlights several characteristics that explain the success of PSO:
-Simple implementation.
-Few control parameters.
-Fast convergence.
-Effective for continuous optimization problems.
-Suitable for nonlinear and multidimensional search spaces.

-Does not require gradient information.
-Adaptable to many engineering and scientific applications.
-Successful in noisy and dynamic environments [41].

2.5.1.2 Limitations Of PSO

-Premature convergence to local optima.
-Performance depends on parameter selection (ω, ϕ_1, ϕ_2).
-Swarm diversity decreases during optimization.
-Performance may deteriorate in highly multimodal problems.
-Convergence speed can slow near the optimum.
-No universal parameter settings exist for all problems.
-Theoretical understanding of swarm behavior remains incomplete [41].

2.5.2 Problem Formulation For Channel Estimation Optimization

The problem of channel estimation is formulated as a weighted sum mean square error (WSMSE) minimisation problem over the pilot symbols and other optimisation variables. It can be seen from this formulation that the mean square error (MSE) of each mobile station (MS) is a function of its path loss. In practical systems it is preferable that the accuracy of the estimation is similar among all users. Hence, a WSMSE objective function is considered, where each MSE term is weighted by the inverse of the corresponding path loss. Thus the optimisation problem can be written as [42]:

$$\min_{\mathbf{x}_k, \mathbf{w}_k, V_k} \sum_{k=1}^{K} \frac{1}{g_k} \xi_k \quad \text{s.t.} \quad \mathbf{x}_k^H \mathbf{x}_k \leq P_k \tag{2.40}$$

$$\mathbf{w}_k^H \mathbf{w}_k \leq P_k \tag{2.41}$$

Furthermore, the problem in (45) can be equivalently reformulated into a more compact form as follows [42]:

$$\min_{V_k} \operatorname{tr} \left\{ \left(\sum_{k=1}^{K} g_k V_k + \sigma^2 I_N \right)^{-1} \right\} \tag{2.42}$$

$$\text{s.t.} \quad \operatorname{tr}(V_k) \leq P_k, \quad V_k \succeq 0, \quad \operatorname{Rank}(V_k) = 1, \quad \forall k \tag{2.43}$$

2.6 Optimization Objectives

2.6.1 MSE Minimization

Loss function is one of the important components in neural networks (NNs), which is used to evaluate the deviation between the predicted outputs of the model and the real target values. The main aim here is to measure the prediction error, which helps the model to improve its performance. During training , the neural network updates the weights and biases iteratively to minimise the loss function . This leads to better predictions[43].

The loss function is also used as an optimisation objective and as an evaluation metric to assess the overall performance of the model. The selection of an appropriate loss function is important in determining the efficiency of training as well as the final predictive accuracy (depending on the nature of the task – regression, classification, etc.

In back propagation the gradient of loss function is calculated and propagated through the network to update the parameters of network. Such mechanism guarantees a gradual reduction of prediction error during training iterations, and hence provides an effective guidance for the learning process.

The Mean Squared Error (MSE) loss function is one of the most popular loss functions for regression problems. It is provided as [43]:

$$\text{MSE} = \frac{1}{n}\sum_{i=1}^{n}(y_i - \hat{y}_i)^2 \tag{2.44}$$

Where n is the number of samples, y_i is the actual value of the i-th sample and $\hat{y}_i$ is the predicted value.

The MSE function computes the square of the difference between the actual value and predicted value and then averages out the squares of the errors for all the samples. One important property is that the squaring operation penalises bigger errors more. Therefore, this model is encouraged to pay attention to correcting the large prediction errors during training.

MSE is a good solution for regression problems where the output is continuous. This provides a clear and interpretable measure of prediction accuracy. One big disadvantage of MSE, however, is that it is sensitive to outliers. Because the loss function squares the errors , the outliers have an outsized influence on the loss value . This may affect the model performance badly when the dataset contains noisy or extreme values[43] .

2.7 Iterative And Low-Complexity Solvers

In modern wireless communication systems, iterative and low-complexity solvers are widely used to efficiently estimate channels, detect signals, and optimise beamforming with reduced computational complexity. In massive MIMO and XL-MIMO systems, conventional optimisation and estimation techniques can be computationally expensive due to the large number of antennas, users, and channel parameters. Therefore, to find near-optimal solutions, iterative algorithms are used, which perform repeated updates instead of direct matrix inversion or exhaustive search procedures. These solvers refine the estimated solution at each iteration until convergence is achieved. Common iterative methods are Gradient Descent (GD), Conjugate Gradient (CG), Alternating Direction Method of Multipliers (ADMM), Approximate Message Passing (AMP), Orthogonal Matching Pursuit (OMP), and Iterative Shrinkage-Thresholding Algorithms (ISTA). Such methods are useful in sparse channel estimation, compressed sensing, beamforming optimisation and hybrid precoding for mmWave and THz communication systems. Low-complexity solvers greatly alleviate the computational burden, memory usage and processing latency, while ensuring acceptable estimation accuracy and spectral efficiency. However, their performances can be dependent on the speed of convergence, initialisation conditions and the selection of parameters [44], [45]

$$x^{(k+1)} = x^{(k)} - \mu\nabla f\left(x^{(k)}\right) \tag{2.45}$$

The iterative low-complexity algorithms are of particular importance in sparse signal recovery and channel estimation problems, as the wireless channels in the massive MIMO and XL-MIMO systems are usually sparse in the angular or spatial domain. Iterative algorithms like Orthogonal Matching Pursuit (OMP) and Approximate Message Passing (AMP) estimate the sparse channel by selecting the most significant components while minimising the reconstruction error. These techniques can significantly reduce pilot overhead and computation complexity than the traditional estimation methods. Furthermore, iterative solvers are frequently integrated with machine learning and Bayesian frameworks to further enhance the convergence performance and estimation accuracy in the future 6G communication systems [46][47].

2.8 Conclusion

This chapter gives an overview of the key channel estimation and optimisation methods applied in Massive MIMO and XL-MIMO communication systems. Classical estimators, e.g., LS and LMMSE, are simple and effective solutions. Compressed sensing-based approaches exploit the channel sparsity to decrease the pilot overhead and computational complexity. The use of the prior statistical and physical channel knowledge further improves the estimation performance by Bayesian and parametric methods. In addition, machine learning and deep learning techniques have become an effective tool to learn complex channel characteristics and improve estimation performance in dynamic environments.

Chapter 3

Simulation Results and Performance Evaluation

Chapter 3

Simulation Results and Performance Evaluation

3.1 Introduction

This chapter provides a comprehensive numerical evaluation and discussion of the pro posed channel estimation frameworks developed in this work for extremely large-scale MIMO(XL-MIMO)systems. To rigorously assess performance across diverse operational environments, our analyzis is divided into two core investigations. The first part evaluates the proposed Simultaneous Orthogonal Matching Pursuit (SOMP) hybrid scheme, focus ing on its ability to handle multi-user structural joint sparsity across varying electromag netic field boundaries. The second part investigates the challenge of modern near-field de ployments by analyzing the proposed Regularized Orthogonal Matching Pursuit (ROMP) algorithm within a mixed line-of-sight (LoS) and non-line-of-sight (NLoS) framework.

3.2 Channel Estimation in Different Fields for XL MIMO

3.2.1 System and Signal Mode

In an XL-MIMO system, a Base Station (BS) equipped with an N-element extremely large-scale antenna array communicates with a single-antenna user. The received signal model in the downlink for M time slots is formulated as:

$$y = Ph + n \tag{3.1}$$

Where: $y \in \mathbb{C}^{M\times 1}$ is the received pilot vector, $P \in \mathbb{C}^{M\times N}$ is the transmitted pilot matrix, $h \in \mathbb{C}^{N\times 1}$ is the high-dimensional XL-MIMO channel vector, and $n \sim \mathcal{CN}(0, \sigma^2 I_M)$ is the additive white Gaussian noise (AWGN).

To reduce pilot overhead ($M \ll N$), we exploit the sparsity of the channel in specific transform domains.

3.2.2 Channel Modeling Paradigms

The electromagnetic field is divided by the Rayleigh distance ($Z = \frac{2D^2}{\lambda}$), which dictates the appropriate channel model.

3.2.2.1 Far-Field Model

When the distance between the BS and scatters exceeds the Rayleigh distance, the planar wave assumption is used. The channel is modeled as:

$$h_{far} = \sqrt{\frac{N}{L}} \sum_{l=1}^{L} \alpha_l \mathbf{a}(\theta_l) \tag{3.2}$$

where L is the number of path components (effective scatterers) between the BS and the user, while α_l and θ_l denote the complex gain and spatial angle of the l-th path, respectively. Assuming a planar wavefront, the standard far-field array steering vector $\mathbf{a}(\theta_l) \in \mathbb{C}^{N\times 1}$ is expressed as:

$$\mathbf{a}(\theta_l) = \frac{1}{\sqrt{N}} \left[1, e^{-j\pi\theta_l}, \ldots, e^{-j(N-1)\pi\theta_l}\right]^H. \tag{3.3}$$

The channel is sparse in the angle domain using a DFT matrix $\mathbf{F}$, where $\mathbf{F} = [\mathbf{a}(\theta_1), \ldots, \mathbf{a}(\theta_N)] \in \mathbb{C}^{N\times N}$ is a unitary matrix containing mutually orthogonal far-field steering vectors defined as:

$$\theta_n = \frac{2n - N - 1}{N}, \quad n = 1, 2, \ldots, N. \tag{3.4}$$

3.2.2.2 Near-Field Model

For scatters within the Rayleigh distance, the spherical wave assumption must be applied to account for phase variations across the large array aperture. The channel is modeled as:

$$h_{near} = \sqrt{\frac{N}{L}} \sum_{l=1}^{L} \alpha_l \mathbf{b}(\theta_l, r_l) \tag{3.5}$$

Assuming a spherical wavefront propagation profile, the near-field steering vector $\mathbf{b}(\theta_l, r_l) \in \mathbb{C}^{N\times 1}$ for the l-th scattering path is expressed as [6]:

$$\mathbf{b}(\theta_l, r_l) = \frac{1}{\sqrt{N}} \left[e^{-j\frac{2\pi}{\lambda}(r_l^{(1)} - r_l)}, \ldots, e^{-j\frac{2\pi}{\lambda}(r_l^{(N)} - r_l)}\right]^H, \tag{3.6}$$

where r_l represents the physical distance from the l-th scatterer to the reference center of the antenna array. The exact geometric distance from the l-th scatterer to the specific n-th BS antenna element is given by:

$$r_l^{(n)} = \sqrt{r_l^2 + \delta_n^2 d^2 - 2 r_l \delta_n d\theta_l}, \tag{3.7}$$

where d denotes the uniform antenna element spacing, and $\delta_n = \frac{2n-N-1}{2}$ represents the structural index of the n-th antenna element for $n = 1, 2, \ldots, N$.

Sparsity is achieved in the polar domain using a transform matrix $\mathbf{W}$ sampled in both angle and distance, the transform matrix $\mathbf{W}$ is structured as:

$$\mathbf{W} = \left[\mathbf{b}(\theta_1, r_1^1), \ldots, \mathbf{b}(\theta_1, r_1^{S_1}), \ldots, \mathbf{b}(\theta_N, r_N^1), \ldots, \mathbf{b}(\theta_N, r_N^{S_N})\right], \tag{3.8}$$

where each column represents a discrete near-field array steering vector evaluated at a sampled spatial angle θ_n and physical distance $r_n^{s_n}$.

Here, $s_n = 1, 2, \ldots, S_n$, where S_n denotes the total number of discrete range samples selected for the n-th angular grid direction. Consequently, the total dimension of the sampled polar-domain search grid across all angles is defined by

$$S = \sum_{n=1}^{N} S_n \tag{3.9}$$

3.2.2.3 Hybrid-Field Model

A practical XL-MIMO environment is often a hybrid, containing both far-field and near-field path components. The proposed model is:

$$h_{hybrid} = \sqrt{\frac{N}{L}} \left(\sum_{l_f=1}^{\gamma L} \alpha_{l_f} \mathbf{a}(\theta_{l_f}) + \sum_{l_n=1}^{(1-\gamma)L} \alpha_{l_n} \mathbf{b}(\theta_{l_n}, r_{l_n}) \right) \tag{3.10}$$

Where $\gamma \in [0, 1]$ is an adjustable parameter controlling the proportion of far-field vs. near-field components.

3.2.3 Nused Model SOMP-Based Estimation

The idea of the present work is extracted from the work detailled in [48] where we use Simultaneous Orthogonal Matching Pursuit (SOMP) to estimate the hybrid-field channel. SOMP is particularly effective when the channel exhibits a common sparsity pattern across multiple sub-carriers or time slots, allowing for more robust support recovery. The estimation process is divided into two main stages:

1. **Far-Field Support Recovery:** Using the angle-domain sensing matrix $A_f = PF$, SOMP identifies the common support for planar wave components.

2. **Near-Field Support Recovery:** Using the polar-domain sensing matrix $A_n = PW$, the algorithm recovers the remaining spherical wave components while removing the contribution of the already estimated far-field paths from the residual.

To adapt the hybrid-field estimation for a SOMP approach, the algorithm handles multiple measurement vectors (MMVs). This is useful in XL-MIMO where the support remains constant across multiple snapshots, even if path gains vary. Based on the hybrid-field framework, the detailed algorithm is presented below.

Algorithm 7 HF-SOMP Based Hybrid-Field Channel Estimation

InputInput OutputOutput InitInitialization
Received pilot matrix $Y = [y_1, y_2, \ldots, y_T] \in \mathbb{C}^{M \times T}$,
Sensing matrices $A_f = PF$ and $A_n = PW$,
Number of paths L, adjustable parameter γ
Estimated hybrid-field channel matrix $\hat{H}$
$L_f = \gamma L,\ L_n = (1-\gamma)L,\ \Omega_f = \emptyset,\ \Omega_n = \emptyset,\ R_0 = Y$
Stage 1: Estimate far-field path components (Angle Domain)

for $l_f = 1\ L_f$ **do** $g =$ row-wise $\|A_f^H R_{l_f-1}\|_2^2$
$n^* = \arg\max_{n \in \{1,\ldots,N\}} \{g_n\}$
$\Omega_f = \Omega_f \cup \{n^*\}$
$\hat{H}_A(\Omega_f, :) = (A_f(:, \Omega_f))^\dagger Y$
$R = Y - A_f(:, \Omega_f)\hat{H}_A(\Omega_f, :)$
Stage 2: Estimate near-field path components (Polar Domain)

for $l_n = 1\ L_n$ **do**
$g =$ row-wise $\|A_n^H R\|_2^2$
$n^* = \arg\max_{n \in \{1,\ldots,S\}} \{g_n\}$
$\Omega_n = \Omega_n \cup \{n^*\}$
$\hat{H}_P(\Omega_n, :) = (A_n(:, \Omega_n))^\dagger (Y - A_f \hat{H}_A)$

if $\Omega_f \neq \emptyset$ **then** $R = Y - A_f\hat{H}_A - A_n(:, \Omega_n)\hat{H}_P(\Omega_n, :)$

else $R = Y - A_n(:, \Omega_n)\hat{H}_P(\Omega_n, :)$
Stage 3: Channel Reconstruction
$\hat{H} = F\hat{H}_A + W\hat{H}_P$
return $\hat{H}$

3.2.4 Simulation

To validate the performance of the proposed two-stage hybrid-field channel estimation framework, comprehensive numerical simulations are conducted. We consider an XL-MIMO system operating at a carrier frequency of 30 GHz ($\lambda = 0.01$ m) where the Base Station (BS) is equipped with a uniform linear array (ULA) of $N = 512$ antennas. The specific channel parameters and system configurations are detailed in Table I.

Table 3.1: Simulation Parameters

Parameter	**Operational Definition**	**Value**
N	Number of BS Antennas	512
f_c	Carrier Frequency	30 GHz
λ	Carrier Wavelength	0.01 m
L	Total Number of Paths	6
α_l	Complex Path Gain	$\alpha_l \sim \mathcal{CN}(0, 1)$
θ_l	Spatial Angle of Departure	$\theta_l \sim \mathcal{U}(-1, 1)$
r_l	Physical Path Distance	$r_l \sim \mathcal{U}(10, 80)$ m
S	Polar-Domain Grid Sample Size	2071
M	Pilot Length (CS / LS Schemes)	256
M_{MMSE}	Pilot Length (MMSE Benchmark)	512 ($P = I_N$)
$\mathbf{P}$	Pilot Matrix Elements	Randomly from $\left\{-\frac{1}{\sqrt{M}}, +\frac{1}{\sqrt{M}}\right\}$

The proposed Hybrid-Field Simultaneous Orthogonal Matching Pursuit (HF-SOMP) channel estimation scheme is evaluated against four classical baseline schemes:

1. Far-Field SOMP Scheme which employs standard angular-domain discrete Fourier transform (DFT) dictionaries.
2. Near-Field SOMP Scheme which uses a polar-domain transform matrix built entirely over the sampled grid space ($S = 2071$).
3. Ideal MMSE Estimator which serves as the optimal theoretical benchmark, simulated under full pilot overhead ($M = 512$) with an identity pilot matrix ($\mathbf{P} = \mathbf{I}_N$).
4. Least Squares (LS) Estimator which serves as the standard non-parametric baseline, estimated directly under the same compressed pilot overhead without leveraging any sparse spatial dictionaries.

3.2.4.1 Result Analysis

To evaluate the estimation accuracy of the various algorithms, the performance metric employed is the Normalized Mean Square Error (NMSE), which is analytically defined as:

$$\text{NMSE} = \mathbb{E}\left[\frac{\|\mathbf{H} - \widehat{\mathbf{H}}\|_F^2}{\|\mathbf{H}\|_F^2}\right] \tag{3.11}$$

where $\widehat{\mathbf{H}}$ denotes the estimated channel matrix, $\|\cdot\|_F$ represents the Frobenius norm, and $\mathbb{E}[\cdot]$ denotes the statistical expectation operator. Furthermore, to ensure statistical stability, each numerical data point presented in the performance evaluation figures is averaged over 300 independent Monte Carlo channel realizations.

1-NMSE Performance vs. SNR

Fig.3.1 presents the NMSE performance comparison as a function of the operational SNR ranging from 0 to 10 dB, simulated under the baseline parameters detailed in the text ($N = 512$, $L = 6$, and compressed pilot overhead $M = 256$).

The Proposed hybrid-field SOMP scheme outperforms all simulated baselines including Far-field SOMP, Near-field SOMP, and the non-parametric LS estimator across the entire SNR range, confirming its superior structural accuracy. From Fig.3.1, we can observe that as the SNR increases, the estimation errors of the sparse recovery algorithms and the LS estimator decrease linearly.

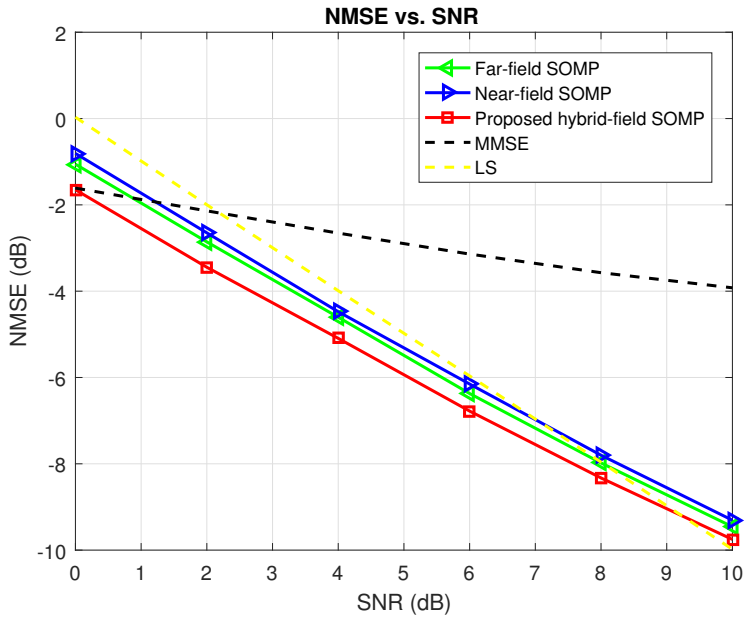


Figure 3.1: NMSE performance comparison with respect to the SNR.

2-NMSE Performance vs. Number of Paths

Fig.3.2 plots the NMSE performance as a function of the total number of propagation paths (L), simulated under a fixed configuration of SNR $= 5$ dB and pilot overhead $M = 256$.

The Proposed hybrid-field SOMP scheme outperforms both the Far-field SOMP and Near-field SOMP frameworks across the entire simulated path range, validating its structural accuracy under varying channel complexities. As the number of paths increases from 2 to 10, the NMSE of all sparse recovery algorithms degrades. This degradation occurs because a higher path count increases multi-path interference and structural leakage within a fixed pilot length ($M = 256$), straining the compressed sensing recovery matrix. When the environment becomes dense ($L \geq 8$), standard Far-field and Near-field SOMP schemes lose their sparse modeling advantages and perform worse than the non-parametric LS baseline. .

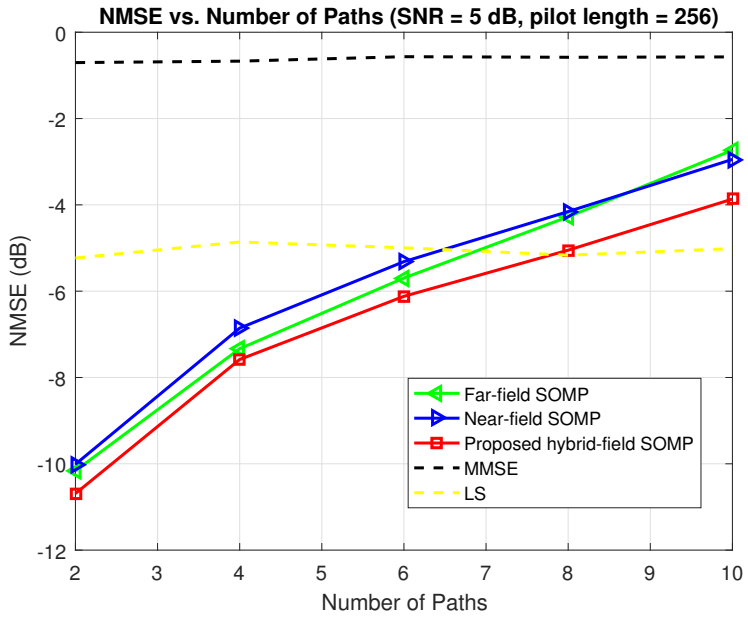


Figure 3.2: NMSE performance comparison with respect to the Number of Paths

3-NMSE Performance vs. Pilot Overhead

Fig.3.3 evaluates the NMSE performance as a function of the pilot overhead (M), simulated under an SNR = 5 dB and $L = 6$ physical paths. The Proposed hybrid-field SOMP scheme maintains a distinct accuracy advantage, consistently achieving the lowest NMSE across the entire simulated range of pilot lengths ($M = 200$ to 300).In addition, as the pilot overhead expands, the NMSE of all sparse recovery techniques decreases steadily.

The proposed scheme operating with a highly compressed pilot size of $M = 200$ still outperforms both standard Far-field and Near-field SOMP configurations operating at their maximum pilot overhead ($M = 300$). This highlights its superior pilot efficiency and robust modeling capacity against structural leakage, while remaining securely bounded well below the optimal baseline thresholds.

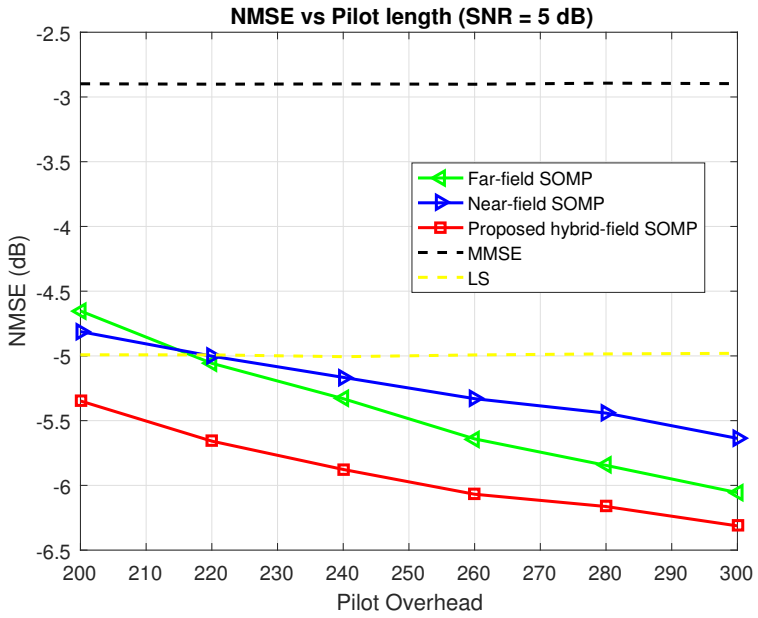


Figure 3.3: NMSE performance comparison with respect to the Pilot Overhead

4-NMSE Performance vs. Sparsity Level

Fig.3.4 illustrates the NMSE performance across different assumed sparsity levels given $L = 6$ physical paths at SNR $= 5$ dB. The Proposed hybrid-field SOMP scheme consistently achieves the lowest NMSE across all sparsity configurations, successfully validating its ability to simultaneously model near-field and far-field spatial characteristics. For all sparse recovery algorithms, the NMSE degrades when the assumed sparsity level exceeds the true physical path number ($L > 6$). This occurs because overestimation forces the dictionary to pick up noisy, redundant grid components.

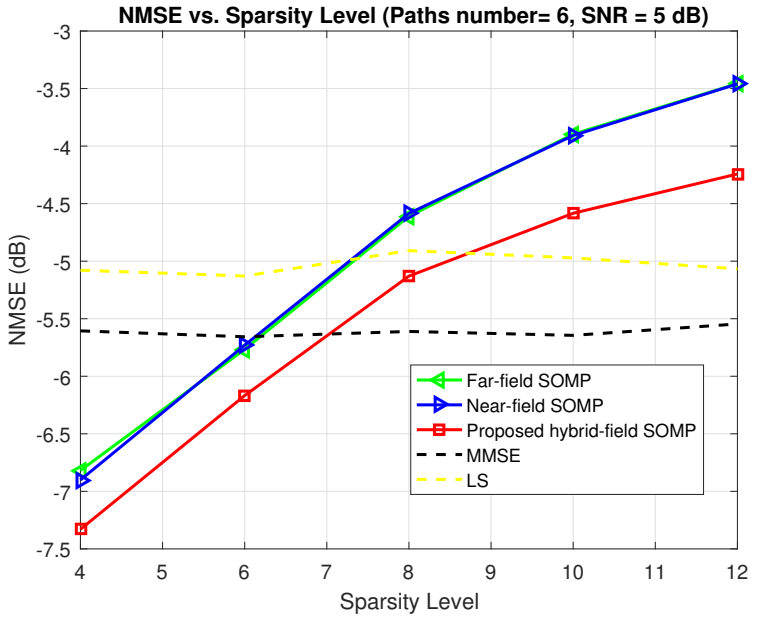


Figure 3.4: NMSE performance comparison with respect to the Sparsity Level

5-NMSE Performance vs. Adjustable Parameter

Fig.3.5 evaluates the NMSE performance against the adjustable parameter γ, which controls the proportion of far-field components ($\gamma = 0$ corresponds to a pure near-field channel, while $\gamma = 1$ denotes a pure far-field channel), under $L = 6$, SNR $= 5$ dB, and $M = 256$.

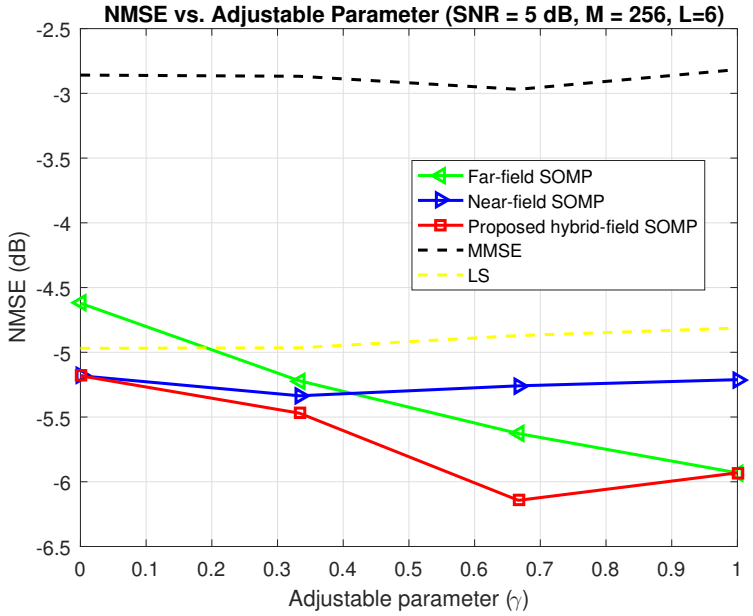


Figure 3.5: NMSE performance comparison with respect to the Adjustable Parameter

The Proposed hybrid-field SOMP scheme successfully unifies both field paradigms. When $\gamma = 0$, it converges precisely to the performance of the pure Near-field SOMP baseline. Conversely, when $\gamma = 1$, it achieves the exact same NMSE as the pure Far-field SOMP scheme, analytically validating its architectural flexibility. Across all intermediate hybrid states ($0 < \gamma < 1$), the proposed algorithm consistently achieves the lowest NMSE, reaching its optimal performance near $\gamma = 0.67$ where it maintains a robust gap above the LS and MMSE benchmarks.

3.3 Exploiting Mixed LoS/NLoS Environments for Near-Field Channel Estimation in XL-MIMO Systems

To enable ultra-high spectral efficiency in 6G networks, this work addresses the limitations of existing extremely large-scale MIMO (XL-MIMO) channel models, which fail to capture mixed line-of-sight (LoS) and non-line-of-sight (NLoS) propagation in the emerging near-field region. We propose a decoupled mixed LoS/NLoS near-field channel model, rigorously deriving the MIMO-RD and MIMO-ARD boundaries to define the hybrid-field zones. Based on this framework, a highly accurate two-stage channel estimation algorithm is introduced: it first isolates and refines the geometric LoS parameters via iterative optimization, and subsequently recovers the NLoS paths using a specialized Regularized Orthogonal Matching Pursuit (ROMP) estimator that exploits polar-domain sparsity.

3.3.1 System and Signal Model

We consider a hybrid digital-analog extremely large-scale MIMO (XL-MIMO) system where the transmitter and receiver are equipped with N_1-element and N_2-element antenna arrays, respectively (see Fig.3.6). To constrain hardware costs, the system uses a limited number of radio frequency (RF) chains, denoted as $N_{\mathrm{t}}^{\mathrm{RF}}$ at the transmitter and $N_{\mathrm{r}}^{\mathrm{RF}}$ at the receiver.

Let $\mathbf{H} \in \mathbb{C}^{N_2 \times N_1}$ represent the hybrid-field channel matrix. During the m-th time slot, the transmitted pilot block $\mathbf{s}_m \in \mathbb{C}^{N_{\mathrm{t}}^{\mathrm{RF}} \times 1}$ is processed by the hybrid precoding matrix $\mathbf{Q} \in \mathbb{C}^{N_1 \times N_{\mathrm{t}}^{\mathrm{RF}}}$, yielding the transmitted spatial signal vector $\mathbf{p}_m = \mathbf{Q}\mathbf{s}_m \in \mathbb{C}^{N_1 \times 1}$. After passing through the channel, the signal is collected at the receiver via the combining matrix $\mathbf{W} \in \mathbb{C}^{N_{\mathrm{r}}^{\mathrm{RF}} \times N_2}$. The received signal vector $\mathbf{y}_m \in \mathbb{C}^{N_{\mathrm{r}}^{\mathrm{RF}} \times 1}$ for a single time slot is expressed as:

$$\mathbf{y}_m = \mathbf{WHQ}\mathbf{s}_m + \mathbf{n}_m, \tag{3.12}$$

where $\mathbf{n}_m \sim \mathcal{CN}(\mathbf{0}, \sigma^2 \mathbf{I}_{N_{\mathrm{r}}^{\mathrm{RF}}})$ represents the complex additive white Gaussian noise (AWGN) vector with variance σ^2. By aggregating the received signals over M consecutive time slots within a channel coherence interval, the complete observation model can be compactly written in matrix form as:

$$\mathbf{Y} = \mathbf{WHP} + \mathbf{N}, \tag{3.13}$$

where $\mathbf{Y} = [\mathbf{y}_1, \mathbf{y}_2, \ldots, \mathbf{y}_M] \in \mathbb{C}^{N_{\mathrm{r}}^{\mathrm{RF}} \times M}$ is the total received measurement block, $\mathbf{P} = [\mathbf{p}_1, \mathbf{p}_2, \ldots, \mathbf{p}_M] \in \mathbb{C}^{N_1 \times M}$ is the overall pilot transmission matrix, and $\mathbf{N} = [\mathbf{n}_1, \mathbf{n}_2, \ldots, \mathbf{n}_M] \in \mathbb{C}^{N_{\mathrm{r}}^{\mathrm{RF}} \times M}$ denotes the total noise matrix distributed as $\mathbf{N} \sim \mathcal{CN}(\mathbf{0}, \sigma^2 \mathbf{I}_{N_{\mathrm{r}}^{\mathrm{RF}}} \otimes \mathbf{I}_M)$. Given the massive scale of the transmitter array (N_1), the channel estimation framework is designed to accurately reconstruct $\mathbf{H}$ from the known matrices $\mathbf{Y}$, $\mathbf{W}$, and $\mathbf{P}$ while maintaining a low-overhead regime ($M < N_1$).

3.3.2 Characterization of Mixed LoS/NLoS Near-Field Channels

To simultaneously capture the distinctive physical features of both LoS and NLoS propagation, we propose a comprehensive, mixed LoS/NLoS near-field XL-MIMO channel model. Combining the geometric free-space LoS formulation and the spherical-wave NLoS path components, the complete channel matrix $\mathbf{H} \in \mathbb{C}^{N_2 \times N_1}$ is formulated as:

$$\mathbf{H} = \mathbf{H}_{\mathrm{LoS}} + \mathbf{H}_{\mathrm{NLoS}} = \mathbf{H}_{\mathrm{LoS}}(r, \theta, \varphi) + \mathbf{D}_r \left(\sum_{l=1}^{L} g_l \mathbf{b}(\theta_r^l, d_r^l) \mathbf{b}^H(\theta_t^l, d_t^l) \right) \mathbf{D}_t^H, \tag{3.14}$$

where the deterministic LoS matrix $\mathbf{H}_{\mathrm{LoS}}(r, \theta, \varphi)$ accounts for absolute spherical phase distortions across the massive array aperture. Specifically, by utilizing the exact geometric relationship in free space, each entry of the LoS matrix is expressed as:

$$\mathbf{H}_{\mathrm{LoS}} = \left[\frac{1}{r_{n_2,n_1}} e^{-j\frac{2\pi}{\lambda} r_{n_2,n_1}} \right]_{N_2 \times N_1}, \tag{3.15}$$

where r_{n_2,n_1} represents the precise geometric distance between the n_1-th transmitter antenna element and the n_2-th receiver antenna element. Here, r denotes the baseline distance between the first antenna element of both arrays, while θ and φ represent the physical angle of departure (AoD) and the relative alignment angle between the receiver

and transmitter arrays, respectively. The structural phase profiles are scaled by the antenna spacing parameters $d_1 = n_1 d$ and $d_2 = n_2 d$, with d representing the uniform element spacing.

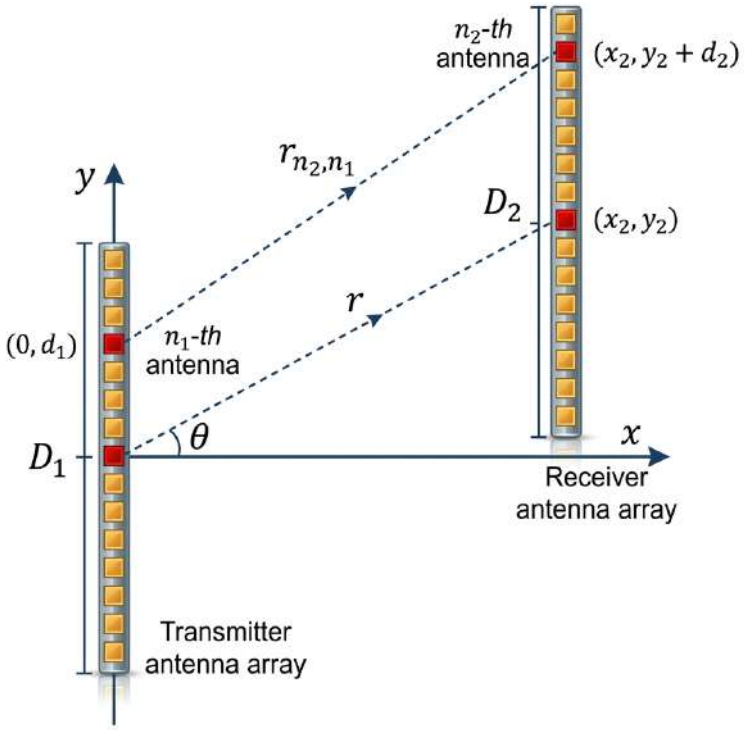


Figure 3.6: Geometric structure of a near-field XL-MIMO system with both transmitter and receiver equipped by uniform linear arrays

3.3.3 Rayleigh Distance Boundaries for Near-Field XL-MIMO

To establish clear operational boundaries for the proposed mixed LoS/NLoS channel model, it is essential to define the geometric regions governing wavefront propagation. As illustrated in Fig.3.7, the spatial continuum is partitioned into three distinct operational fields based on two critical metric thresholds: the MIMO Advanced Rayleigh Distance (MIMO-ARD) and the conventional MIMO Rayleigh Distance (MIMO-RD).

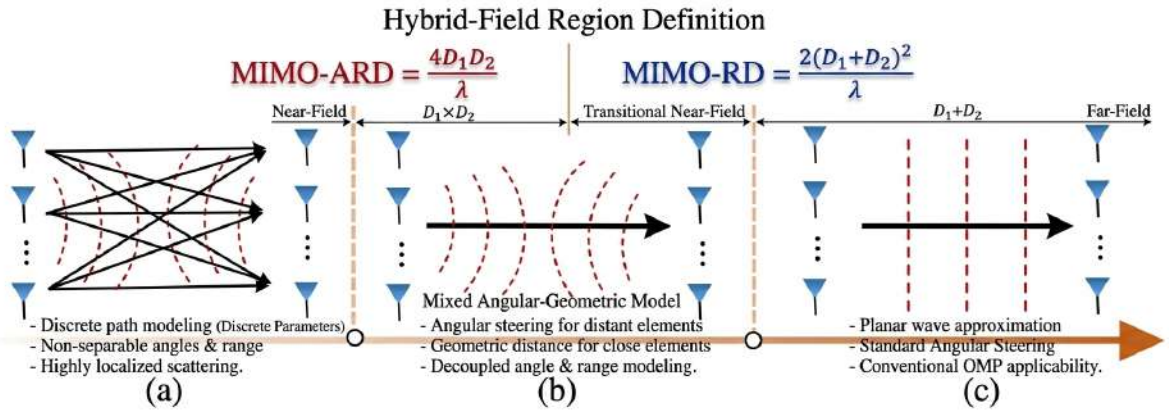


Figure 3.7: Definition of propagation regions: (a) Extreme near-field zone, (b) Transitional near-field zone, and (c) Conventional planar far-field zone

A. MIMO Advanced Rayleigh Distance (MIMO-ARD) In conventional near-field sparse channel paradigms, both the LoS and NLoS path components are typically modeled via the direct product of dual independent near-field array response vectors. To define the boundary where the cross-array phase interactions become highly non-separable, the MIMO Advanced Rayleigh Distance (MIMO-ARD) is defined as [222]:

$$\text{MIMO-ARD} = \frac{4D_1D_2}{\lambda}, \tag{3.16}$$

where D_1 and D_2 denote the physical apertures of the transmitter and receiver antenna arrays, respectively, and λ represents the carrier wavelength.

B. MIMO Rayleigh Distance (MIMO-RD) As the transmission distance increases past the advanced threshold, the phase variations stabilize into a more structured pattern. To delineate the final boundary where near-field spherical wave phenomena completely vanish, the comprehensive MIMO Rayleigh Distance (MIMO-RD) is applied:

$$\text{MIMO-RD} = \frac{2(D_1 + D_2)^2}{\lambda}. \tag{3.17}$$

3.3.4 Proposed Near-Field codebook based ROMP

The main idea of this proposition is based on the work of [49], where their authors give an OMP near-field codebook to estimate channel estimation. In our work, we suggest a new method called Regularized Orthogonal Matching Pursuit (ROMP)for near field channel estimation. Here are the ROMP algorithmic steps for specifically tailored for near-field channel estimation using an angle-range polar codebook.

In near-field XL-MIMO, the dictionaries A_1 and A_2 are constructed using polar-domain steering vectors (parameterized by both angle θ and range r) instead of standard far-field angular steering vectors.

Algorithm 8 Regularized Orthogonal Matching Pursuit (ROMP) for Near-Field XL-MIMO Channel Estimation

Input: Received pilot matrix $\mathbf{Y}$, combining matrix $\mathbf{W}$, pilot matrix $\mathbf{P}$, near-field polar-domain codebooks $\mathbf{U}_{n1}$ and $\mathbf{U}_{n2}$, channel path sparsity target T, convergence threshold ϵ.

Initialization:

Initial residual matrix: $\mathbf{R}_0 = \mathbf{Y}$

Initial support index set: $\Omega_0 = \emptyset$

Precomputed effective measurement dictionaries: $_1 = \mathbf{W}\mathbf{U}_{n2}$ and $_2 = \mathbf{U}_{n1}^H\mathbf{P}$

for $t = 1$ to T **do**

Match Filtering (Correlation):

Compute the space-correlation matrix mapping the discrete angle-range polar grid:

$$\mathbf{M}_t = {}_1^H\mathbf{R}_{t-1}\,{}_2^H$$

Vectorize the grid response:

$$\mathbf{v} = \mathrm{vec}(\mathbf{M}_t)$$

Identify Largest Components:

Find the index set J_0 corresponding to the J largest elements in magnitude from v, where:

$$J = \min(2T, \mathrm{length}(\mathbf{v}))$$

Regularization Gate:

Find all subsets $I \subset J_0$ such that for any two coordinates i,$j \in \mathcal{I}$:

$$|v(i)| \leq 2|v(j)|$$

Select the optimal regularized subset I_{best} that carries the maximum aggregate energy:

$$I_{\text{best}} = \arg\max_I \|\mathbf{v}(I)\|_2^2$$

Support Set Update:

merge the newly regularized off-grid /on-grid atomic coordinates into the active support set:

$$\Omega_t = \Omega_{t-1} \cup I_{\text{best}}$$

Least Squares Projection: construct the active dictionary $_{\Omega_t}$ and solve for the sparse path coefficient vector $\mathbf{x}_{\Omega_t}$:

$$\mathbf{x}_{\Omega_t} = (\,{}_{\Omega_t}^H\,{}_{\Omega_t})^{-1}\,{}_{\Omega_t}^H\mathrm{vec}(\mathbf{Y})$$

Residual Matrix Update: reconstruct the estimated sparse channel matrix $\mathbf{X}_t$ from $\mathbf{x}_{\Omega_t}$ and update the remaining signal energy:

$$\mathbf{R}_t = \mathbf{Y} - {}_1\mathbf{X}_t\,{}_2$$

Convergence Check

if $\|\mathbf{R}_t\|_F^2 < \epsilon$ **then**

break

end if

end for

Output: Reconstructed near-field XL-MIMO channel matrix

$$\hat{\mathbf{H}} = \mathbf{U}_{n2}\mathbf{X}_t\mathbf{U}_{n1}^H$$

=0

3.3.5 Proposed Far-Field codebook based ROMP

The main mathematical difference from the near-field version is that the dictionaries U_{f1} and U_{f2} are standard far-field angular DFT matrices (parameterized only by the

Angle of Arrival/Departure θ, assuming planar wavefronts without range variables).

Algorithm 9 Regularized Orthogonal Matching Pursuit (ROMP) for Far-Field Massive MIMO Channel Estimation

Input: Received pilot matrix $\mathbf{Y}$, combining matrix $\mathbf{W}$, pilot matrix $\mathbf{P}$, far-field angular-domain DFT codebooks $\mathbf{U}_{f1}$ and $\mathbf{U}_{f2}$, channel path sparsity target T, convergence threshold ϵ.

Initialization:

Initial residual matrix: $\mathbf{R}_0 = \mathbf{Y}$

Initial support index set: $\Omega_0 = \emptyset$

Precomputed effective measurement dictionaries: $_1 = \mathbf{W}\mathbf{U}_{f2}$ and $_2 = \mathbf{U}_{f1}^H\mathbf{P}$

for $t = 1$ to T **do**

Match Filtering (Correlation):

Compute the space-correlation matrix mapping the discrete angular DFT grid:

$$\mathbf{M}_t = {}_1^H\mathbf{R}_{t-1}\,{}_2^H$$

Vectorize the angular grid response:

$$\mathbf{v} = \mathrm{vec}(\mathbf{M}_t)$$

Identify Largest Components:

Find the index set J_0 corresponding to the J largest elements in magnitude from $\mathbf{v}$, where:

$$J = \min(2T, \mathrm{length}(\mathbf{v}))$$

Regularization Gate:

Find all subsets $I \subset J_0$ such that for any two coordinates $i, j \in I$:

$$|v(i)| \leq 2\,|v(j)|$$

Select the optimal regularized subset I_{best} that carries the maximum aggregate angular energy:

$$I_{\text{best}} = \arg\max_I \|\mathbf{v}(I)\|_2^2$$

Support Set Update:

Merge the newly regularized angular atomic coordinates into the active support set:

$$\Omega_t = \Omega_{t-1} \cup I_{\text{best}}$$

Least Squares Projection:

Construct the active dictionary $_{\Omega_t}$ and solve for the sparse path coefficient vector x_{Ω_t}:

$$x_{\Omega_t} = (\,{}_{\Omega_t}^H\,{}_{\Omega_t})^{-1}\,{}_{\Omega_t}^H\mathrm{vec}(\mathbf{Y})$$

Residual Matrix Update:

Reconstruct the estimated sparse channel matrix $\mathbf{X}_t$ from x_{Ω_t} and update the remaining signal energy:

$$\mathbf{R}_t = \mathbf{Y} - {}_1\mathbf{X}_t\,{}_2$$

Convergence Check:

if $\|\mathbf{R}_t\|_F^2 < \epsilon$ **then**

break

end if

end for

Output: Reconstructed far-field MIMO channel matrix:

$$\hat{\mathbf{H}} = \mathbf{U}_{f2}\mathbf{X}_t\mathbf{U}_{f1}^H$$

3.3.6 Simulation

In this section, we conduct comprehensive computer simulations to verify the performance of the proposed hybrid-field channel estimation algorithm within the XL-MIMO framework. We consider a system architecture where a Base Station (BS) equipped with a Uniform Linear Array (ULA) operates under a mixed propagation environment containing both far-field and near-field components.

The simulation parameters are configured as follows: the BS is equipped with $N_1 = 256$ antennas, the receiver features $N_2 = 128$ antennas, and the operating frequency is set to $f = 50$ GHz, which corresponds to a wavelength of $\lambda = 0.006$ m. The hybrid-field channel is composed of both far-field and near-field path components, with the total number of physical paths set to $L = 3$. The spatial angles follow a uniform distribution $\mathcal{U}\left(-\frac{\pi}{3}, \frac{\pi}{3}\right)$, while the scatterer distances are randomly generated within the range of $[50, 500]$ meters. To demonstrate its superior estimation accuracy and pilot efficiency, our proposed algorithm, which modifies and unifies the selection rules for both fields, is evaluated against the existing near-field codebook-based OMP method and the conventional far-field codebook-based OMP method. Furthermore, the Cramér-Rao Lower Bound (CRLB) is included in the performance analysis to serve as the absolute theoretical benchmark algorithm.

3.3.6.1 Result Analysis

1- NMSE Performance vs. Transmit-Receive Distance:

Fig.3.8 illustrates the Normalized Mean Square Error (NMSE) performance of the evaluated channel estimation algorithms as a function of the transmit-receive (Tx-Rx) separation distance, varying from $50m$ to $500m$. To comprehensively evaluate the field-mismatch boundaries, the performance curves are analyzed across three distinct geometric regions separated by the MIMO Aperture-Rayleigh Distance ($MIMO-ARD \approx 196.6m$) and the traditional MIMO Rayleigh Distance ($MIMO-RD \approx 442.7\ m$).

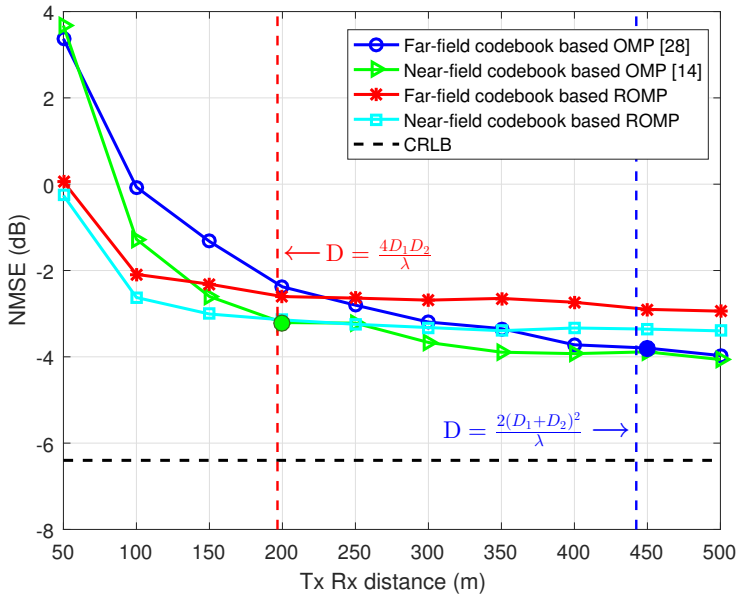


Figure 3.8: Impact of Tx-Rx distance on NMSE performance in XL-MIMO fields.

Fig.3.8 results demonstrate a clear three-region behavior separated by the MIMO-

ARD ($196.6m$) and MIMO-RD ($442.7m$) boundaries. In the extreme near-field, spherical wave dominant region, far-field estimators fail due to severe model mismatch, whereas our proposed modified Near-field codebook-based ROMP effectively captures the phase variations, outperforming standard near-field OMP by up to $2dB$ thanks to its enhanced regularization scheme. As the distance increases through the transition zone, wavefronts flatten, causing the performance of near-field and far-field estimators to steadily converge in the Fraunhofer far-field region at approximately $-4dB$, while the CRLB remains the absolute theoretical baseline at $-6.4dB$.

2- NMSE Performance vs. SNR under varying distances:

Figures 3.9 and 3.10 evaluate the Normalized Mean Square Error (NMSE) performance against the Signal-to-Noise Ratio (SNR) varying from 0 dB to 10 dB with a fixed pilot length of 72, analyzed at distances of 30 m and 90 m, respectively.

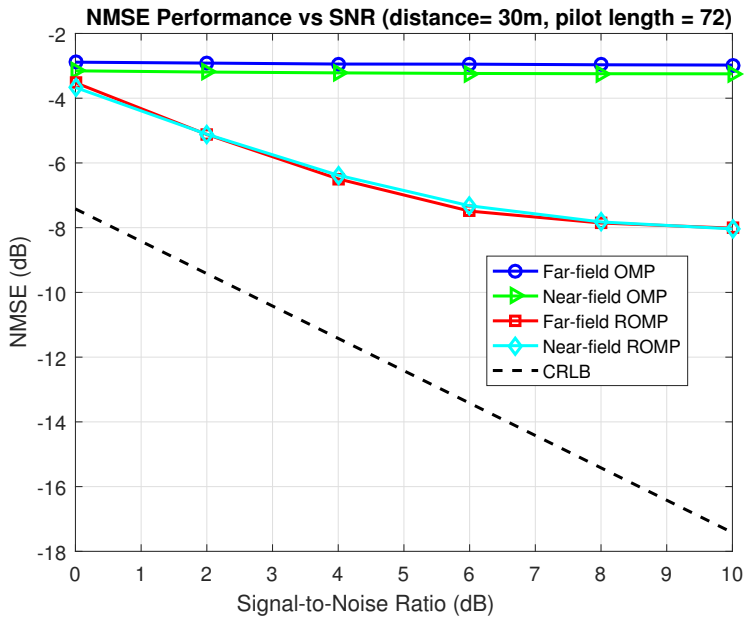


Figure 3.9: NMSE performance vs. SNR under an extreme near-field channel condition (Distance = 30 m, Pilot Length = 72).

At Distance=$30m$ (Fig.3.9): Deep within the extreme near-field region, the geometric structure dominates. Standard OMP algorithms remain entirely trapped at a high NMSE floor of $-3dB$ across the full SNR range due to severe grid mismatch and spherical wave phase distortions. Conversely, both proposed Far-field ROMP and Near-field ROMP display superior tracking capabilities right from $0dB$, steadily decreasing down to $-8dB$ and closely mirroring the downward trajectory of the theoretical CRLB baseline.

At Distance=$90m$ (Fig.3.10): As the distance increases toward the transitional boundary, the behavior shifts. In the low SNR region (0 to 6 dB), standard OMP algorithms outperform the ROMP variants because the regularization stage inside ROMP is highly sensitive to severe noise, leading to initial structural selection errors. However, as the SNR increases beyond $7dB$, the noise power drops, allowing the proposed Far-field ROMP and Near-field ROMP to overcome this noise threshold, scale cleanly downward, and significantly bypass the stagnant floors of conventional OMP methods.

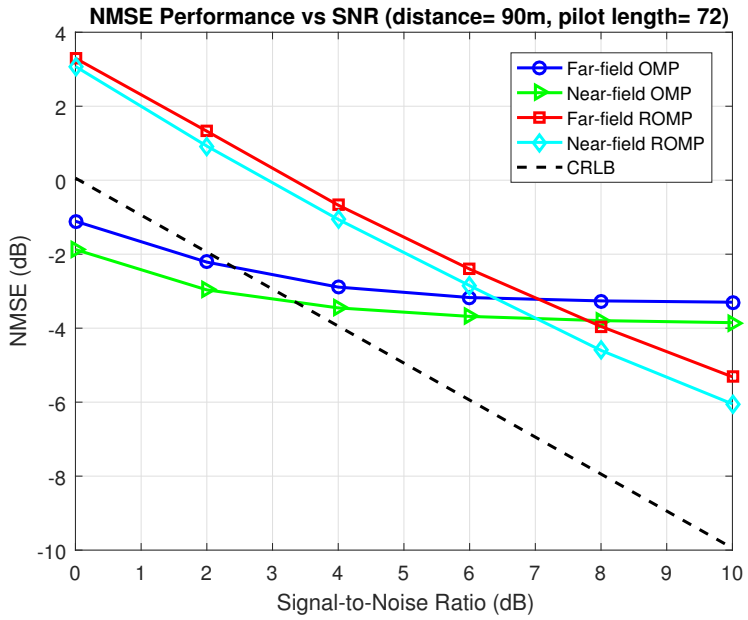


Figure 3.10: NMSE performance vs. SNR under a transitional near-field channel condition (Distance = 90 m, Pilot Length = 72).

3- NMSE Performance vs. Pilot Overhead:

Fig.3.11 illustrates the Normalized Mean Square Error (NMSE) performance of the evaluated estimators as a function of the length of the pilot overhead, sweeping from 40 to 96 at a fixed distance of $50m$ and an SNR=$10dB$.

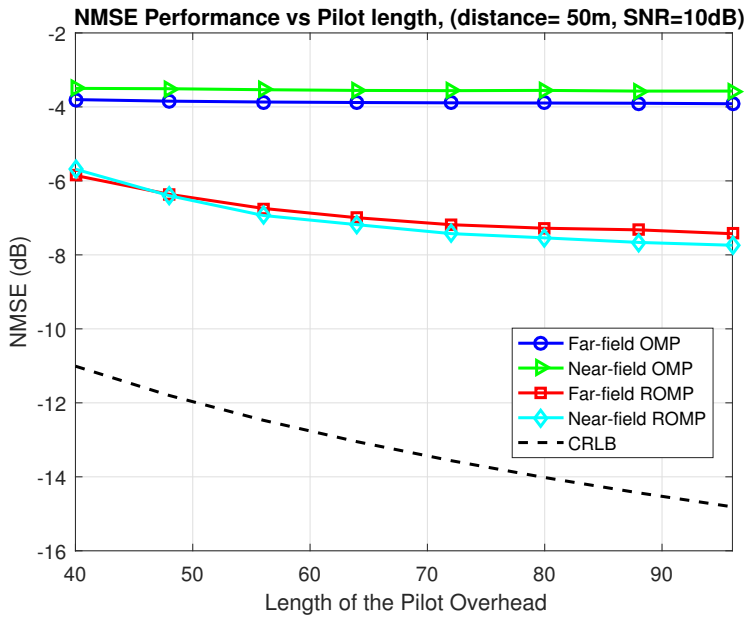


Figure 3.11: Impact of pilot overhead scaling on the estimation accuracy of OMP and proposed ROMP algorithms in XL-MIMO fields.

The simulation results indicate that standard far-field and near-field OMP algorithms suffer from performance stagnation, trapped at a high NMSE floor of approximately $-4dB$ due to grid mismatch issues that cannot be resolved by adding more pilots. Conversely, the

proposed regularized algorithms (Far-field ROMP and Near-field ROMP) scale efficiently with the observation size, showing continuous improvement as the NMSE drops from $-5.8dB$ to nearly $-8dB$. Driven by its specialized support selection rules, Near-field ROMP achieves the highest accuracy by successfully tracking the downward trajectory of the CRLB theoretical baseline within this extreme close-range (50 m) setup.

3.4 Conclusion

In this chapter, the performance of the proposed channel estimation algorithms for XL-MIMO systems was thoroughly simulated, analyzed, and discussed.

In the first part of the study, the SOMP hybrid framework demonstrated excellent capabilities in leveraging joint-spatial sparsity, maintaining a low pilot overhead while adapting dynamically to the transitional boundaries between different field regions.

In the second part, the proposed mixed LoS/NLoS near-field ROMP framework successfully addressed the critical issue of grid mismatch. By decoupling the absolute geometric free-space LoS path from the polar-domain sparse NLoS paths, the algorithm achieved better performance compared to the conventional OMP algorithm.

General Conclusion

the thesis we have studied the channel estimation problem in massive MIMO and XL-MIMO systems for 5G and future 6G wireless communications. In the future, wireless networks will be characterised by larger antenna arrays, higher frequency bands and more stringent performance requirements, which will require efficient channel estimation as a fundamental requirement to achieve reliable and high capacity communications.

The paper first discussed the evolution from 5G to 6G communication systems and emphasised the importance of Massive MIMO technology, beamforming techniques and advanced propagation environments. We also reviewed the properties of wireless channels and issues with accurate CSI acquisition.

A comprehensive review of the channel estimation and optimisation techniques was provided. Classical estimators like LS and LMMSE were compared to state-of-the-art and compressed sensing based techniques like OMP, CoSaMP, AMP, GAMP and SAMP. These approaches exploit the channel sparsity to enhance the estimation accuracy at the cost of pilot overhead and computational complexity.

Finally, we conducted extensive simulation studies for XL-MIMO channel estimation scenarios. The obtained results showed the efficiency of optimization-based sparse recovery techniques in improving the performance of channel estimation. In particular, the proposed SOMP framework efficiently utilised the joint sparsity characteristics, and the ROMP-based near-field estimation scheme effectively overcame the grid mismatch problem of traditional OMP methods. The simulation results show that the proposed algorithms outperform the existing ones in terms of NMSE values and more accurate channel reconstruction under different propagation environments.

Finally, the results validate the potential of optimization-based and compressed sensing-based channel estimation techniques for future Massive MIMO and XL-MIMO communication systems. Future work can also be the extension of these approaches by the integration of the artificial intelligence, deep learning techniques and advanced hybrid-field channel models to further improve the estimation accuracy and adaptability in the upcoming 6G wireless networks.

Bibliography

[1] M. S. Alam *et al.*, "Evolution of Wireless Communication Networks from 5G to 6G: Future Perspective," *Radioelectronics and Communications Systems*, vol. 66, no. 5, 2023.

[2] J. Park, S. Samarakoon, H. Shiri, M. K. Abdel-Aziz, T. Nishio, A. Elgabli, and M. Bennis, "Extreme Ultra-Reliable and Low-Latency Communication," *Nature Electronics*, vol. 5, no. 3, pp. 133–141, 2022.

[3] M. S. Alam, S. T. Siddiqui, K. A. Qidwai, A. Aftab, M. S. Kamal, and F. I. Shahi, "Evolution of Wireless Communication Networks from 5G to 6G: Future Perspective," *Radioelectronics and Communications Systems*, vol. 66, no. 5, pp. 213–222, 2023.

[4] V. R. Chintha, Er. Priyanshi, and S. Vashishtha, "NMSE Performance versus Adjustable Parameter γ," *International Journal of Research and Analytical Reviews (IJRAR)*, vol. 7, no. 1, Feb. 2020, ISSN: 2348-1269 (Online), 2349-5138 (Print).

[5] D. P. Bertsekas, *Nonlinear Programming*, 3rd ed. Belmont, MA, USA: Athena Scientific, 2016.

[6] S. Boyd and L. Vandenberghe, *Convex Optimization*. Cambridge, U.K.: Cambridge University Press, 2004.

[7] E. G. Larsson, O. Edfors, F. Tufvesson, and T. L. Marzetta, "Massive MIMO for Next Generation Wireless Systems," *IEEE Communications Magazine*, vol. 52, no. 2, pp. 186–195, Feb. 2014.

[8] Z. Gao, L. Dai, D. Mi, Z. Wang, M. A. Imran, and M. Shakir, "MmWave Massive-MIMO-Based Wireless Backhaul for the 5G Ultra-Dense Network," *IEEE Wireless Communications*, vol. 22, no. 5, pp. 13–21, Oct. 2015.

[9] R. Chataut and R. Akl, "Massive MIMO Systems for 5G and Beyond Networks—Overview, Recent Trends, Challenges, and Future Research Direction," *Sensors*, vol. 20, no. 10, p. 2753, 2020. doi: 10.3390/s20102753.

[10] S. Alraih, I. Shayea, M. Behjati, R. Nordin, N. F. Abdullah, A. Abu-Samah, and D. Nandi, "Revolution or Evolution? Technical Requirements and Considerations towards 6G Mobile Communications," *Sensors*, vol. 22, no. 3, p. 762, 2022. doi: 10.3390/s22030762.

[11] M Meegle, "Massive MIMO Beamforming in 6G." [Online]. Available: https://www.meegle.com/en_us/topics/massive-mimo/massive-mimo-beamforming-in-6g

[12] T. K. Engda, Y. Wondie, and J. Steinbrunn, "Massive MIMO, mmWave and mmWave-Massive MIMO Communications: Performance Assessment with Beamforming Techniques," *Research Square*, 2020. doi:10.21203/rs.3.rs-69959/v1.

[13] B. Ning, Z. Tian, W. Mei, Z. Chen, C. Han, S. Li, J. Yuan, and R. Zhang, "Beamforming Technologies for Ultra-Massive MIMO in Terahertz Communications," *IEEE Open Journal of the Communications Society*, 2023. doi: 10.1109/OJCOMS.2023.3245669.

[14] A. K. Gupta *et al.*, "Propagation Characteristics of Millimeter-Wave and Terahertz Frequencies in 6G Beyond Systems," *ResearchGate*, 2023.

[15] RF Wireless World, "Flat Fading vs. Frequency Selective Fading." [Online]. Available: https://www.rfwireless-world.com/Terminology/flat-fading-vs-frequency-selective-fading.html

[16] M. S. Miah, M. M. Rahman, T. K. Godder, B. C. Singh, and M. T. Parvin, "Performance Comparison of AWGN, Flat Fading and Frequency Selective Fading Channel for Wireless Communication System using 4QPSK," *International Journal of Computer and Information Technology (IJCIT)*, vol. 1, no. 2, pp. 82–90, 2011.

[17] M. Olyaee, H. Hashemi, and J. M. Romero Jerez, "Channel Fading Models for 5G and 6G," in *5G and 6G Enhanced Broadband Communications*, IntechOpen, 2024. doi:10.5772/intechopen.1005006.

[18] S. F. Cotter and B. D. Rao, "Sparse Channel Estimation via Matching Pursuit with Application to Equalization," *IEEE Transactions on Communications*, vol. 50, no. 3, pp. 374–377, Mar. 2002.

[19] Wu, Y., "Machine Learning Algorithms for 5G PUCCH Channel Estimation," Master's thesis, Aalto University, Finland, 2023.

[20] Antonio Assalini, Emiliano Dall'Anese, and Silvano Pupolin, "Linear MMSE MIMO Channel Estimation with Imperfect Channel Covariance Information," in *Proceedings of the IEEE International Conference on Communications (ICC)*, IEEE, 2009.

[21] C. R. Berger, Z. Wang, J. Huang, and S. Zhou, "Application of Compressive Sensing to Sparse Channel Estimation," Carnegie Mellon University and University of Connecticut.

[22] J. A. Tropp and A. C. Gilbert, "Signal Recovery From Random Measurements Via Orthogonal Matching Pursuit," *IEEE Transactions on Information Theory*, vol. 53, no. 12, pp. 4655–4666, Dec. 2007.

[23] Y. C. Pati, R. Rezaiifar, and P. S. Krishnaprasad, "Orthogonal Matching Pursuit: Recursive Function Approximation with Applications to Wavelet Decomposition," in *Proceedings of the 27th Asilomar Conference on Signals, Systems and Computers*, Pacific Grove, CA, USA, Nov. 1993, pp. 40–44.

[24] W. Dai and O. Milenkovic, "Subspace Pursuit for Compressive Sensing Signal Reconstruction," *IEEE Transactions on Information Theory*, vol. 55, no. 5, pp. 2230–2249, May 2009.

[25] D. Needell and J. A. Tropp, "CoSaMP: Iterative Signal Recovery from Incomplete and Inaccurate Samples," *Applied and Computational Harmonic Analysis*, vol. 26, no. 3, pp. 301–321, May 2009.

[26] J. Gao, C. Zhong, X. Chen, H. Lin, and G. Y. Li, "AMP-SBL Unfolding for Wideband mmWave Massive MIMO Channel Estimation," *arXiv preprint arXiv:2302.00461*, 2023.

[27] S. Rangan, "Generalized Approximate Message Passing for Estimation with Random Linear Mixing," *arXiv preprint arXiv:1010.5141v2*, Aug. 2012.

[28] X. Wang, Y. Jiang, and G. Ding, "An Improved Variable Step SAMP Method Based on Correlation Principle," *Sensors*, vol. 22, no. 19, 2022.

[29] T. L. Marzetta, E. G. Larsson, H. Yang, and H. Q. Ngo, *Fundamentals of Massive MIMO*. Cambridge, United Kingdom: Cambridge University Press, 2016.

[30] S. M. Kay, *Fundamentals of Statistical Signal Processing: Estimation Theory*. Upper Saddle River, NJ, USA: Prentice Hall, 1993.

[31] P. Tarafder, C. Chun, A. Ullah, Y. Kim, and W. Choi, "Channel Estimation in 5G-and-Beyond Wireless Communication: A Comprehensive Survey," *Electronics*, vol. 14, no. 4, p. 750, 2025.

[32] A. F. Molisch, *Wireless Communications*, 2nd ed. Hoboken, NJ, USA: Wiley–IEEE Press, 2011.

[33] T. L. Marzetta, E. G. Larsson, H. Yang, and H. Q. Ngo, *Fundamentals of Massive MIMO*. Cambridge, U.K.: Cambridge University Press, 2016.

[34] R. O. Schmidt, "Multiple Emitter Location and Signal Parameter Estimation," *IEEE Transactions on Antennas and Propagation*, vol. 34, no. 3, pp. 276–280, Mar. 1986.

[35] R. Roy and T. Kailath, "ESPRIT—Estimation of Signal Parameters via Rotational Invariance Techniques," *IEEE Transactions on Acoustics, Speech, and Signal Processing*, vol. 37, no. 7, pp. 984–995, Jul. 1989.

[36] A. M. Sayeed, "Deconstructing Multiantenna Fading Channels," *IEEE Transactions on Signal Processing*, vol. 50, no. 10, pp. 2563–2579, Oct. 2002.

[37] S. M. Kay, *Fundamentals of Statistical Signal Processing: Estimation Theory*. Englewood Cliffs, NJ, USA: Prentice Hall, 1993.

[38] E. J. Candès and M. B. Wakin, "An Introduction to Compressive Sampling," *IEEE Signal Processing Magazine*, vol. 25, no. 2, pp. 21–30, 2008.

[39] A. T. Cemgil, "Bayesian Inference for Nonnegative Matrix Factorisation Models," *Computational Intelligence and Neuroscience*, vol. 2009, Article ID 785152, 2009.

[40] H. Ye, G. Y. Li, and B.-H. Juang, "Deep Learning Based Channel Estimation in Massive MIMO Systems," *IEEE Transactions on Wireless Communications*, vol. 18, no. 10, pp. 4885–4898, 2019.

[41] R. Poli, J. Kennedy, and T. Blackwell, "Particle Swarm Optimization: An Overview," *Swarm Intelligence*, vol. 1, no. 1, pp. 33–57, 2007.

[42] T. E. Bogale and L. B. Le, "Pilot Optimization and Channel Estimation for Multiuser Massive MIMO Systems," *arXiv preprint arXiv:1402.0045*, 2014.

[43] A. V. Oppenheim and G. C. Verghese, *Signals, Systems and Inference*. MIT OpenCourseWare, Massachusetts Institute of Technology, 2010.

[44] S. Boyd and L. Vandenberghe, *Convex Optimization*. Cambridge, United Kingdom: Cambridge University Press, 2004.

[45] Y. Nesterov, *Introductory Lectures on Convex Optimization: A Basic Course*. Boston, MA, USA: Springer, 2004.

[46] J. A. Tropp and A. C. Gilbert, "Signal Recovery From Random Measurements Via Orthogonal Matching Pursuit," *IEEE Transactions on Information Theory*, vol. 53, no. 12, pp. 4655–4666, Dec. 2007.

[47] Z. Gao, L. Dai, S. Han, C.-L. I, and R. W. Heath Jr., "Energy-Efficient Hybrid Analog and Digital Precoding for MmWave MIMO Systems With Large Antenna Arrays," *IEEE Journal on Selected Areas in Communications*, vol. 34, no. 4, pp. 998–1009, Apr. 2016.

[48] Y. Lu and L. Dai, "Channel Estimation for Extremely Large-Scale Massive MIMO: Far-Field, Near-Field, or Hybrid-Field?" *IEEE Communications Letters*, vol. 26, no. 1, pp. 177–181, Jan. 2022.

[49] Y. Lu and L. Dai, "Near-Field Channel Estimation in Mixed LoS/NLoS Environments for Extremely Large-Scale MIMO Systems," *IEEE Transactions on Communications*, vol. 71, no. 6, pp. 3694–3707, Jun. 2023.